PHILOSOPHICAL TRANSACTIONS OF THE ROYAL SOCIETY A MATHEMATICAL, PHYSICAL & ENGINEERING SCIENCES

The Stress Distribution near a Loading Point in a Uniform Flanged Beam

E. W. Parkes

Phil. Trans. R. Soc. Lond. A 1952 **244**, 417-467
doi: 10.1098/rsta.1952.0011

THE STRESS DISTRIBUTION NEAR A LOADING POINT IN A UNIFORM FLANGED BEAM

By E. W. PARKES

Engineering Department, University of Cambridge

(*Communicated by Sir Geoffrey Taylor, F.R.S.—Received* 15 *August* 1951)

CONTENTS

	PAGE
NOTATION	417
INTRODUCTION	419
PART I. BEAM LOADED THROUGH THE WEB	420
1. The incompatibilities in engineers' theory	420
2. Self-equilibrating stress systems applied to a finite length of beam	422
3. Combination of self-equilibrating stress systems to compensate for the errors in engineers' theory	425
4. A numerical example	430
5. General considerations	436
PART II. BEAM LOADED THROUGH THE FLANGES	438
6. Equal and opposite loads on the flanges	438
6·1. Introduction	438
PART II (cont.)	PAGE
6·2. Flange resting on a semi-infinite plate	439
6·3. Beam of finite depth	445
6·4. Effects of various parameters	448
7. Equal and similar loads on the flanges	451
8. Full analysis applied to a numerical example	452
PART III. EXPERIMENTAL EVIDENCE	454
9. Experimental results	454
10. Statistical analysis of the results	457
PART IV. COMPARISON OF THE ANALYSES OF THE PRESENT PAPER WITH OTHER RECENT WORK	464
11. Taylor's analysis	464
12. Winny's analysis	466
REFERENCES	467

The elementary theory of bending, which is the method by which the stresses in a uniform flanged beam subjected to transverse loading are usually determined, leads to certain incompatibilities of displacement and stress distribution near a section of the beam at which load is applied. The present paper endeavours to remedy these deficiencies. Two main cases are considered: that in which the beam is loaded through the web and that in which it is loaded through the flanges. In both of these the analyses lead to stress concentrations in the outer fibres of the flanges, and it is found that the maximum stress concentrations, which occur at the loading section, may be expressed with an accuracy sufficient for most engineering purposes by means of simple formulae. For both cases, maximum concentration factors occur in short beams having large flanges and thin webs.

Results of strain-gauge tests carried out on mild steel beam specimens are presented which show very good agreement between the predicted and experimental stress distributions in the flanges, and a further part of the paper compares the present analyses with other recent work on the subject.

NOTATION

A_b	area of boom
C, D	coefficients in stress functions
E	Young's modulus
F	function in Fourier's integral theorem
F_s	statistical function

G	shear modulus
H	semi-depth of beam
I	second moment of area of beam
I_b	second moment of area of boom about its own neutral axis
J	$\left\{\frac{(1+\nu)\,(3-\nu)}{2}\frac{I_b}{t_w}\right\}^{\frac{1}{3}}$
K	function in Winny's analysis
L	semi-span of beam
M	applied bending moment at any section
M_b	bending moment in the boom at any section
P_b	end load in the boom at any section
Q	value of $q(x)$
R_1	strain-gauge reading when beam is subjected to pure bending
R_2	strain-gauge reading when beam is subjected to any other loading
S	applied shear at any section
S_b	shear in the boom at any section
T	shear stress at the origin
U	$\int_0^{2h/n} u\,dy$ at $x=0$
$T_1 \ldots T_4$, U_2, U_4	symbols defining exponential stress systems
W	load applied to beam or to a flange
a	distance from web attachment to neutral axis of boom
b	distance from neutral axis of boom to outermost fibre
c	$\frac{J}{(1/Q+x)}$
d	$\left\lvert\frac{J}{1/Q-x}\right\rvert$
eng.	suffix denoting engineers' theory
exp.	suffix denoting exponential stress system
f, g	non-dimensional functions defining stress concentration in outermost fibre
h	semi-depth of web between web-boom attachments
k	function in Winny's analysis
l	length of beam considered in analysis
m	odd integer defining harmonic stress system
n	integer defining exponential stress system
p	number of experimental points
q	experimental standard deviation
$q(x)$	normal loading
r	percentage change of resistance of strain gauge
$r_{\text{tot.}}$	total range of r
sss	suffix denoting superimposed stress system
t	thickness of boom or web
t_s	'Student's' statistical ratio

PHILOSOPHICAL TRANSACTIONS OF THE ROYAL SOCIETY A MATHEMATICAL, PHYSICAL & ENGINEERING SCIENCES

t_w	thickness of web
u, v	displacements in the directions of x and y
u_b, v_b	displacements of boom at $y = h$
u_w, v_w	displacements of web at $y = h$
w	load increments
x, y	co-ordinate axes
z	$x\eta/2J$
Γ	value of σ_y at $x = 0, y = h$
Λ	maximum value of τ_{xy} at $y = h$
$\Gamma_1 \dots \Gamma_5$ $\Lambda_1 \dots \Lambda_5$	symbols defining harmonic stress systems
Ψ	stress concentration factor
α, β	decay or frequency factors in stress functions
ζ	function defined in part II
η	αJ
θ	slope of regression line
λ	coefficient of variation
μ	number of strain gauge readings
ν	Poisson's ratio
ξ	constant in regression line equation
ρ	experimental arithmetic mean
σ_x, σ_y	direct stresses
$(\sigma_x)_H$	outer fibre stress
$(\sigma_x)_s$	stress concentration—i.e. stress in excess of that given by engineers' theory
τ_{xy}	shear stress
ϕ	stress function
χ	function in Fourier's integral theorem
ψ	universe standard deviation
units:	Lb. and in. unless otherwise stated

INTRODUCTION

The elementary theory of the bending of beams (known in the aircraft industry, as 'engineers' theory') suggests that the direct stresses at any section of a uniform beam are proportional to the applied bending moment. For sections remote from points of load application this theory gives accurate predictions of the stresses and displacements. Near a loading section, however, it is necessary to investigate the problem in greater detail.

In recent years Taylor (1949) and Winny (1950) have offered approximate solutions. Taylor considered a beam subjected to two equal loads, applied to each flange, and by assuming the web to be shear-carrying only obtained the direct stresses in the flanges from the equations for compatibility of horizontal and vertical displacement at the web-boom† junction. Winny used a somewhat similar method, but introduced the vertical compressibility of the web and the stiffness of the rivets joining it to the flanges.

† The words 'boom' and 'flange' are synonymous.

The present paper is more comprehensive than the previous ones in that it considers both load applied entirely to the web and any combination of load applied to the flanges. The web is considered as an isotropic plate capable of carrying direct and shear stresses. In the case of web loading, an approximate stress-function method is used, the stresses being everywhere compatible but the strains at the web-boom junction only approximately so. The analyses for flange loading are exact within the limits of the assumptions.

The paper is divided into four main parts: the analysis for web loading; the analysis for flange loading; experimental work; and a comparison of the results with those of Taylor and Winny.

PART I. BEAM LOADED THROUGH THE WEB

1. The incompatibilities in engineers' theory

We consider a uniform flanged beam, symmetrical about its neutral axis, having the dimensions shown in figure 1. At some section of the beam, taken for convenience as our origin of co-ordinates, there is applied a transverse load W. Then, since we assume that at sections remote from points of application of load, engineers' theory gives a close approximation to the stress distribution, we may without loss of generality apply temporary loads (to be removed later) at sections far from W, such that the shear forces in the beam on either side of W are $S = \pm\frac{1}{2}W$. The overall bending moment due to W at any section of the beam will be taken as M, and it follows that $S = -\partial M/\partial x$. Then according to the elementary theory of bending the stress system (which throughout the paper will be considered to be two-dimensional) is given by

$$\left.\begin{aligned} \sigma_x &= \frac{M}{I}y, \\ \sigma_y &= 0, \\ \tau_{xy} &= -\frac{S}{It}\int_y^H ty\,\mathrm{d}y. \end{aligned}\right\} \tag{1}$$

On applying this stress system to the web (treated as a flat rectangular plate) we obtain the appropriate displacements as

$$\left.\begin{aligned} u &= \int_0^x \frac{My}{EI}\,\mathrm{d}x - \frac{Sy(h^2-y^2)}{6GI}, \\ v &= -\int_0^x\int_0^x \frac{M}{EI}\,\mathrm{d}x\,\mathrm{d}x - \frac{\nu My^2}{2EI} - \frac{S}{Gt_wI}\left\{A_b(a+h)+\frac{t_wh^2}{3}\right\}x, \end{aligned}\right\} \tag{2}$$

our rigid-body conditions being that u and v are zero at the origin and u is zero at $x = 0$, $y = h$.

The boom displacements, by similar methods, are obtained as

$$\left.\begin{aligned} u &= \int_0^x \frac{My}{EI}\,\mathrm{d}x - \frac{S}{GI}\int_h^y \frac{1}{t}\int_y^H ty\,\mathrm{d}y\,\mathrm{d}y + \frac{S(y-h)}{GI(a+b)}\int_h^H \frac{1}{t}\int_y^H ty\,\mathrm{d}y\,\mathrm{d}y, \\ v &= -\int_0^x\int_0^x \frac{M}{EI}\,\mathrm{d}x\,\mathrm{d}x - \frac{\nu My^2}{2EI} - \frac{Sx}{GI(a+b)}\int_h^H \frac{1}{t}\int_y^H ty\,\mathrm{d}y\,\mathrm{d}y, \end{aligned}\right\} \tag{3}$$

the rigid-body conditions being $u = 0$ at $x = 0$, $y = h$ and H, and $v_{\text{boom}} = v_{\text{web}}$ at $x = 0$, $y = h$.

By inserting practical figures in equation (3) it will be found that the boom displacement terms in S are quite negligible both compared with those in M and with those in S in equation (2). Accordingly, it will be sufficiently accurate to take the boom displacements as

$$\left.\begin{aligned} u &= \int_0^x \frac{My}{EI}\,\mathrm{d}x, \\ v &= -\int_0^x \int_0^x \frac{M}{EI}\,\mathrm{d}x\,\mathrm{d}x - \frac{\nu My^2}{2EI}, \end{aligned}\right\} \tag{4}$$

a result which would be achieved by treating the boom as a beam obeying the elementary theory of bending and using the rigid-body conditions $u = \partial v/\partial x = 0$† and $v_{\text{boom}} = v_{\text{web}}$ at $x = 0$. In future we shall in fact treat the boom by this method, an approximation which can be justified arithmetically at any time by investigating the magnitude of the shear distortion terms as given by equation (3).

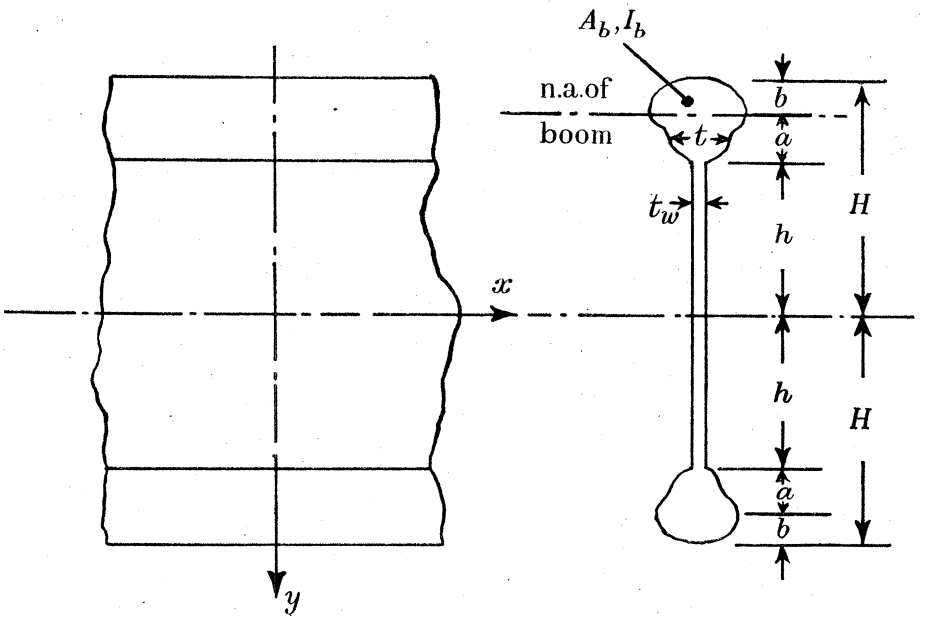

FIGURE 1. Dimensions of beam.

Comparing equations (2) and (4) it may be seen that at the junction of boom and web the u displacements are compatible, but the v displacements leave a gap

$$v_w - v_b = -\frac{S}{Gt_w I}\left\{A_b(a+h) + \frac{t_w h^2}{3}\right\} x. \tag{5}$$

At the centre line of the beam ($x = 0$), u_{web} is zero at $y = 0$ and h, but elsewhere has values

$$u_{\text{web}} = -\frac{Sy(h^2 - y^2)}{6GI}. \tag{6}$$

Engineers' theory of bending thus leads to incompatibilities of vertical displacement at the junction of boom and web and of horizontal displacement at the centre line of the beam (the loading section).‡ In addition, the distribution of shear associated with this theory is

† Strictly, $\partial v/\partial x = \nu Sy^2/2EI$, but the difference from zero is negligible.
‡ Auxiliary calculations have shown that of these two errors the former is by far the more important.

untrue at the loading section. The load W will be applied by means of a patch plate attached to the centre portion of the web, and the shear stress in the outer portions of the web and in the booms will be zero.

In the following sections of the paper we endeavour to develop an analysis to remove these incompatibilities of displacement and load distribution. As above, we shall treat the boom as a beam obeying the simple engineers' theory stresses and displacements and the web as a flat rectangular plate obeying the general elasticity equations for plane stress.

2. Self-equilibrating stress systems applied to a finite length of beam

As a means of compensating for the errors inherent in engineers' theory of bending, we consider the application of self-equilibrating stress systems to the finite length of the web between $x = 0$ and $x = l$, where l is for the moment an arbitrary parameter. We shall use the trigonometric solutions of the stress-function equation, and these fall into two main types, those leading to an exponential loading between web and boom and those leading to a harmonic loading.

The first type may be represented by the function

$$\phi = \sin \alpha y (C_1 \cosh \alpha x + C_2 \sinh \alpha x + C_3 x \cosh \alpha x + C_4 x \sinh \alpha x) \tag{7}$$

($\cos \alpha y$ terms are zero from considerations of symmetry), where

$$\alpha = \frac{n\pi}{2h}, \tag{8}$$

giving rise to the stress system

$$\left.\begin{aligned}
\sigma_x &= -\alpha^2 \sin \alpha y \{C_1 \cosh \alpha x + C_2 \sinh \alpha x + C_3 x \cosh \alpha x + C_4 x \sinh \alpha x\}, \\
\sigma_y &= \sin \alpha y \{C_1 \alpha^2 \cosh \alpha x + C_2 \alpha^2 \sinh \alpha x + C_3 \alpha (2 \sinh \alpha x + \alpha x \cosh \alpha x) \\
&\qquad + C_4 \alpha (2 \cosh \alpha x + \alpha x \sinh \alpha x)\}, \\
\tau_{xy} &= -\alpha \cos \alpha y \{C_1 \alpha \sinh \alpha x + C_2 \alpha \cosh \alpha x + C_3 (\cosh \alpha x + \alpha x \sinh \alpha x) \\
&\qquad + C_4 (\sinh \alpha x + \alpha x \cosh \alpha x)\}.
\end{aligned}\right\} \tag{9}$$

Then if the portion of the web beyond $x = l$ is not to be loaded (a desirable condition for self-equilibrium) it is necessary that

$$\sigma_x = \tau_{xy} = 0 \quad \text{at} \quad x = l, \tag{10}$$

i.e. that
$$C_1 \cosh \alpha l + C_2 \sinh \alpha l + C_3 l \cosh \alpha l + C_4 l \sinh \alpha l = 0 \tag{11}$$

and
$$C_1 \alpha \sinh \alpha l + C_2 \alpha \cosh \alpha l + C_3 (\cosh \alpha l + \alpha l \sinh \alpha l) + C_4 (\sinh \alpha l + \alpha l \cosh \alpha l) = 0. \tag{12}$$

Further, if the shear stress at the origin is to be T,

$$-C_2 \alpha^2 - C_3 \alpha = T. \tag{13}$$

We now have three equations for the determination of the coefficients $C_1 \ldots C_4$. For our remaining condition we must consider two cases. First, if n is even, σ_y is zero at $x = l$, $y = h$ (ideally σ_y should be zero everywhere at $x = l$ to agree with engineers' theory, but in practice we content ourselves with ensuring that it is so at the most important point, the web-

boom junction), and we use the remaining equation to impose a known displacement at the centre line of the beam. This displacement is conveniently expressed by its integral

$$E\int_0^{2h/n} u\,dy = U, \tag{14}$$

whence

$$-\frac{2}{\alpha}\{C_2\alpha(1+\nu)-C_3(1-\nu)\} = U. \tag{15}$$

Secondly, if n is odd, σ_y is not necessarily zero at $x = l$, $y = h$, and we use our final equation to make it so,

$$C_1\alpha^2\cosh\alpha l + C_2\alpha^2\sinh\alpha l + C_3\alpha(2\sinh\alpha l+\alpha l\cosh\alpha l) + C_4\alpha(2\cosh\alpha l+\alpha l\sinh\alpha l) = 0. \tag{16}$$

From equations (11), (12), (13) and (15) the coefficients are obtained as (n even)

$$\left.\begin{aligned}
C_1 &= \frac{1}{4\alpha^2(\alpha l+\sinh\alpha l\cosh\alpha l)}[T\{2(1+\nu)\,\alpha^2l^2+2(1-\nu)\sinh^2\alpha l\}+U\alpha^2\{\sinh^2\alpha l-\alpha^2l^2\}],\\
C_2 &= \frac{1}{4\alpha^2}[-T\{2(1-\nu)\}-U\alpha^2],\\
C_3 &= \frac{1}{4\alpha}[-T\{2(1+\nu)\}+U\alpha^2],\\
C_4 &= \frac{1}{4\alpha(\alpha l+\sinh\alpha l\cosh\alpha l)}[T\{2(1-\nu)+2(1+\nu)\cosh^2\alpha l\}-U\alpha^2\{\sinh^2\alpha l\}],
\end{aligned}\right\} \tag{17}$$

and from equations (11), (12), (13) and (16) as (n odd)

$$\left.\begin{aligned}
C_1 &= \frac{T(\alpha l\cosh\alpha l-\sinh\alpha l)}{\alpha^3l\sinh\alpha l},\\
C_2 &= \frac{T(\cosh\alpha l-\alpha l\sinh\alpha l)}{\alpha^3l\sinh\alpha l},\\
C_3 &= \frac{-T\cosh\alpha l}{\alpha^2l\sinh\alpha l},\\
C_4 &= \frac{T}{\alpha^2l}.
\end{aligned}\right\} \tag{18}$$

Having evaluated the coefficients C_1, C_2, C_3 and C_4, the displacements may be determined. (We use the same rigid-body conditions as previously, $u = v = 0$ at the origin, $u = 0$ at $x = 0$, $y = h$.) In particular, at $x = 0$

$$Eu = \{C_2\alpha(1+\nu)-C_3(1-\nu)\}\left\{\frac{y}{h}\sin\alpha h-\sin\alpha y\right\}, \tag{19}$$

and at $y = h$,

$$\left.\begin{aligned}
Eu_w = &-\sin\alpha h[C_1\alpha(1+\nu)\sinh\alpha x+C_2\alpha(1+\nu)\,(\cosh\alpha x-1)\\
&+C_3\{(1+\nu)\,\alpha x\sinh\alpha x-(1-\nu)\,(\cosh\alpha x-1)\}\\
&+C_4\{(1+\nu)\,\alpha x\cosh\alpha x-(1-\nu)\sinh\alpha x\}],\\
Ev_w = &-\cos\alpha h[C_1\alpha(1+\nu)\cosh\alpha x+C_2\alpha(1+\nu)\sinh\alpha x\\
&+C_3\{2\sinh\alpha x+(1+\nu)\,\alpha x\cosh\alpha x\}\\
&+C_4\{2\cosh\alpha x+(1+\nu)\,\alpha x\sinh\alpha x\}]\\
&+C_1\alpha(1+\nu)+2C_4\\
&-\{C_2\alpha(1+\nu)-C_3(1-\nu)\}\frac{x}{h}\sin\alpha h.
\end{aligned}\right\} \tag{20}$$

We now have the web unloaded at $x = l$, subjected to a known shear (in terms of T) at $x = 0$ and having along its upper and lower edges ($y = \pm h$) certain direct and shear stresses determinable in terms of the coefficients. These latter stresses, multiplied by the web thickness (known in the aircraft industry as fluxes and having the units of Lb./in.) must now be applied to the boom with their signs reversed. The boom, as before, is assumed to be held with zero slope at $x = 0$ and to be a cantilever beam obeying the elementary theory of bending. We find that there is an end-load in the boom

$$P_b = -t_w \alpha \cos \alpha h \{C_1 \cosh \alpha x + C_2 \sinh \alpha x + C_3 x \cosh \alpha x + C_4 x \sinh \alpha x\}, \tag{21}$$

and a bending moment

$$M_b = t_w (a\alpha \cos \alpha h + \sin \alpha h) \{C_1 \cosh \alpha x + C_2 \sinh \alpha x + C_3 x \cosh \alpha x + C_4 x \sinh \alpha x\}. \tag{22}$$

Denoting the boom displacements at $y = h$ by a suffix b

$$\left.\begin{aligned} Eu_b = &-t_w \left[\left\{\frac{1}{A_b} + \frac{a^2}{I_b}\right\} \cos \alpha h + \frac{a}{I_b \alpha} \sin \alpha h\right] \left[C_1 \sinh \alpha x + C_2 (\cosh \alpha x - 1)\right. \\ &\left. + \frac{C_3}{\alpha} (\alpha x \sinh \alpha x - \cosh \alpha x + 1) + \frac{C_4}{\alpha} (\alpha x \cosh \alpha x - \sinh \alpha x)\right], \\ Ev_b = &-\frac{t_w}{I_b} \left[a \cos \alpha h + \frac{\sin \alpha h}{\alpha}\right] \left[\frac{C_1}{\alpha} (\cosh \alpha x - 1) + \frac{C_2}{\alpha} (\sinh \alpha x - \alpha x)\right. \\ &\left. + \frac{C_3}{\alpha^2} \{\alpha x (\cosh \alpha x + 1) - 2 \sinh \alpha x\} + \frac{C_4}{\alpha^2} \{\alpha x \sinh \alpha x - 2 \cosh \alpha x\}\right] + [Ev_w]_{x=0}. \end{aligned}\right\} \tag{23}$$

The complete stress system in web and boom is entirely self-equilibrating, since its only net 'external' effect is to change the distribution of the shear stress at the centre line.

We return now to the second type of stress system (that producing harmonic loading between web and boom) which has only two arbitrary coefficients, since from considerations of symmetry the stress function must this time be chosen in the form

$$\phi = \cos \beta x (D_1 \sinh \beta y + D_2 y \cosh \beta y) \tag{24}$$

(terms in $\sin \beta x$ are ignored since their function, which is to introduce displacements at $x = 0$, has already been fulfilled by the exponential stress systems), where

$$\beta = \frac{m\pi}{2l}, \tag{25}$$

generating the stress system in the web

$$\left.\begin{aligned} \sigma_x &= \cos \beta x \{D_1 \beta^2 \sinh \beta y + D_2 \beta (2 \sinh \beta y + \beta y \cosh \beta y)\}, \\ \sigma_y &= -\beta^2 \cos \beta x \{D_1 \sinh \beta y + D_2 y \cosh \beta y\}, \\ \tau_{xy} &= \beta \sin \beta x \{D_1 \beta \cosh \beta y + D_2 (\cosh \beta y + \beta y \sinh \beta y)\}. \end{aligned}\right\} \tag{26}$$

We may make σ_x and σ_y zero at $x = l$ by choosing

$$m = 1, 3, 5, \ldots, \tag{27}$$

but from the form of the function τ_{xy} cannot then be zero.

If the value of σ_y at $x = 0$, $y = h$ is to be Γ and the shear stress at $y = h$ is to attain a maximum value of Λ, D_1 and D_2 may be evaluated as

$$\left.\begin{aligned} D_1 &= \frac{-\Gamma(\cosh\beta h + \beta h \sinh\beta h) - \Lambda\beta h \cosh\beta h}{\beta^2(\sinh\beta h \cosh\beta h - \beta h)}, \\ D_2 &= \frac{\Gamma\cosh\beta h + \Lambda\sinh\beta h}{\beta(\sinh\beta h \cosh\beta h - \beta h)}. \end{aligned}\right\} \tag{28}$$

This time it is convenient to substitute for the coefficients analytically and we obtain the displacements at $y = h$ as

$$\left.\begin{aligned} Eu_w &= \frac{\sin\beta x}{\beta(\sinh\beta h \cosh\beta h - \beta h)}[\Gamma\{\beta h + \sinh\beta h \cosh\beta h + \nu(\beta h - \sinh\beta h \cosh\beta h)\} \\ &\qquad + \Lambda\{2\sinh^2\beta h\}], \\ Ev_w &= \frac{\cos\beta x}{\beta(\sinh\beta h \cosh\beta h - \beta h)}[\Gamma\{2\cosh^2\beta h\} \\ &\qquad + \Lambda\{\beta h + \sinh\beta h \cosh\beta h + \nu(\beta h - \sinh\beta h \cosh\beta h)\}], \\ &\quad - \frac{1}{\beta(\sinh\beta h \cosh\beta h - \beta h)}[\Gamma\{2\cosh\beta h + (1+\nu)\beta h \sinh\beta h\} \\ &\qquad + \Lambda\{(1+\nu)\beta h \cosh\beta h - (1-\nu)\sinh\beta h\}]. \end{aligned}\right\} \tag{29}$$

u is everywhere zero at $x = 0$ from our decision to use terms in $\cos\beta x$ only.

Applying the reversed fluxes to the boom we find

$$P_b = \frac{-\Lambda t_w \cos\beta x}{\beta}, \tag{30}$$

$$M_b = (\Lambda\beta a - \Gamma)\frac{t_w}{\beta^2}\cos\beta x + \frac{\Gamma t_w}{\beta^2}\beta(l-x)\sin\beta l, \tag{31}$$

whence

$$\left.\begin{aligned} Eu_b &= \frac{t_w \sin\beta x}{\beta^3}\left[\frac{\Gamma a}{I_b} - \frac{\Lambda\beta}{A_b}\left\{1 + \frac{a^2 A_b}{I_b}\right\}\right] - \frac{\Gamma a t_w \sin\beta l}{\beta I_b} x\left(l - \frac{x}{2}\right), \\ Ev_b &= \frac{t_w(1-\cos\beta x)}{\beta^4 I_b}\{\Gamma - \Lambda\beta a\} - \frac{\Gamma t_w \sin\beta l}{\beta I_b}\frac{x^2}{2}\left(l - \frac{x}{3}\right) + [Ev_w]_{x=0}. \end{aligned}\right\} \tag{32}$$

This time the complete stress system in web and boom is not self-equilibrating, since there is a residual shear in the web at $x = l$. We shall in the following section introduce equations ((40) and (41)) to ensure that for the harmonic stress systems as a whole

and

$$\left.\begin{aligned} &\tau_{xy} = 0 \quad \text{at} \quad x = l,\ y = h, \\ &\int_0^h \tau_{xy}\,dy = 0 \quad \text{at} \quad x = l. \end{aligned}\right\} \tag{33}$$

3. Combination of self-equilibrating stress systems to compensate for the errors in engineers' theory

It will be remembered from a previous section of the paper that the errors in engineers' theory which we wished to correct consisted of a gap in the v displacement between web and boom, a warping of the web at the centre line and an unsatisfactory distribution of shear stress at the loading section. The final stresses in which we shall be principally interested will be those in the boom at $x = 0$, and so in correcting the errors of the elementary theory we must endeavour to ensure accurate values for these quantities. The boom stresses depend on $\partial u_b/\partial x$ and $\partial^2 v_b/\partial x^2$ and accordingly in our analysis we shall try to make

u_b and its differentials up to $\partial^2 u_b/\partial x^2$ and v_b and its differentials up to $\partial^3 v_b/\partial x^3$ correct at $x = 0$. In addition, we shall make the web and boom coincident at $x = l$, and in order to correct the warping of the web we shall make $\partial u/\partial y = 0$ at $x = 0$, $y = h$ and $\int_0^h uy\,dy = 0$ at $x = 0$ (this latter is chosen in preference to $\int_0^h u\,dy = 0$, as it seems to offer hope of a better bending moment agreement). The shear-stress distribution at the loading section will be dealt with by making $S_b = 0$ at $x = 0$ ($\tau_{xy} = 0$ at $x = 0$, $y = h$ follows from two of the previous conditions).

We consider first those errors which can be corrected by means of the exponential type of stress systems. At the loading section engineers' theory gives the following values to functions which should from considerations of symmetry or from our load distribution requirements be zero:

$$(1)\quad \frac{\partial v_w}{\partial x} = \frac{-S}{Gt_w I}\left\{A_b(a+h)+\frac{t_w h^2}{3}\right\},$$

$$(2)\quad \left(\frac{\partial u}{\partial y}\right)_{y=h} = \frac{Sh^2}{3GI},$$

These two together, when corrected, ensure that $\tau_{xy} = 0$ at $y = h$

$$(3)\quad \int_0^h uy\,dy = -\frac{Sh^5}{45GI},$$

$$(4)\quad S_b = -\frac{S}{I}\{A_b a(a+h)+I_b\},$$

$$(5)\quad \frac{\partial^2 u_b}{\partial x^2} = -\frac{Sh}{EI},$$

$$(6)\quad \frac{\partial^2 u_w}{\partial x^2} = -\frac{Sh}{EI},$$

$$(7)\quad \frac{\partial^3 v_b}{\partial x^3} = \frac{S}{EI},$$

$$(8)\quad \frac{\partial^3 v_w}{\partial x^3} = \frac{S}{EI}.$$

Numbers 5 and 7 are not independent conditions—they are satisfied provided 1, 2 and 4 are correct.

These errors can all be compensated by the introduction of four exponential stress systems ($n = 1, \ldots, 4$) defined by the symbols (T_1), (T_2, U_2), (T_3) and (T_4, U_4). The equations which must be satisfied are conveniently expressed as follows:

$$S_b = -\frac{S}{I}\{A_b a(a+h)+I_b\}-\frac{2ht_w}{\pi}T_1+\frac{2ht_w}{3\pi}T_3 = 0, \tag{34}$$

$$E\partial^2\frac{(u_w-u_b)}{\partial x^2} = \frac{t_w}{A_b}\left\{1+\frac{a^2A_b}{I_b}\right\}(T_2-T_4)-T_1\left\{\frac{2t_w ah}{\pi I_b}-\frac{\left\{2\nu\cosh\frac{\pi l}{2h}+(1+\nu)\frac{\pi l}{2h}\sinh\frac{\pi l}{2h}\right\}}{l\sinh\frac{\pi l}{2h}}\right\}$$

$$+T_3\left\{\frac{2t_w ah}{3\pi I_b}-\frac{\left\{2\nu\cosh\frac{3\pi l}{2h}+(1+\nu)\frac{3\pi l}{2h}\sinh\frac{3\pi l}{2h}\right\}}{l\sinh\frac{3\pi l}{2h}}\right\} = 0, \tag{35}$$

$$E\left(\frac{\partial u}{\partial y}\right)_{y=h} = \frac{2(1+\nu)\,Sh^2}{3I} - \frac{1}{2}\left(\frac{\pi}{h}\right)^2 (U_2 - 4U_4) + T_1 4h \frac{\left\{2\cosh\frac{\pi l}{2h} - (1+\nu)\frac{\pi l}{2h}\sinh\frac{\pi l}{2h}\right\}}{\pi^2 l \sinh\frac{\pi l}{2h}}$$

$$- T_3 4h \frac{\left\{2\cosh\frac{3\pi l}{2h} - (1+\nu)\frac{3\pi l}{2h}\sinh\frac{3\pi l}{2h}\right\}}{9\pi^2 l \sinh\frac{3\pi l}{h}} = 0, \quad (36)$$

$$E\int_0^h uy\,dy = \frac{-2(1+\nu)\,Sh^5}{45I} + \frac{h}{2}(U_2 - U_4) + T_1 4h^4\left(\frac{1}{3} - \frac{4}{\pi^2}\right)\frac{\left\{2\cosh\frac{\pi l}{2h} - (1+\nu)\frac{\pi l}{2h}\sinh\frac{\pi l}{2h}\right\}}{\pi^2 l \sinh\frac{\pi l}{2h}}$$

$$- T_3 4h^4\left(\frac{1}{3} - \frac{4}{9\pi^2}\right)\frac{\left\{2\cosh\frac{3\pi l}{2h} - (1+\nu)\frac{3\pi l}{2h}\sinh\frac{3\pi l}{2h}\right\}}{9\pi^2 l \sinh\frac{3\pi l}{2h}} = 0, \quad (37)$$

$$G\left(\frac{\partial v_w}{\partial x} - \frac{\partial u}{\partial y}\right) = \frac{-SA_b(a+h)}{t_w I} - T_2 + T_4 = 0, \quad (38)$$

$$\frac{E\partial^3(v_w - v_b)}{\partial x^3} = \left(1+\frac{\nu}{2}\right)\left(\frac{\pi}{h}\right)^4 (U_2 - 16U_4) - (1+\nu)(3+\nu)\left(\frac{\pi}{h}\right)^2 (T_2 - 4T_4) + \frac{ta}{I_b}(T_2 - T_4)$$

$$- \frac{2ht_w}{\pi I_b} T_1 + \frac{2ht_w}{3\pi I_b} T_3 = 0. \quad (39)$$

On substituting equation (38) in equation (35), we have three independent pairs of equations, i.e. (34) and (35) may be solved for T_1 and T_3, then (36) and (37) for U_2 and U_4, and finally (38) and (39) for T_2 and T_4.

Having determined the magnitudes of (T_1), (T_2, U_2), (T_3) and (T_4, U_4) we may evaluate the displacements due to these systems and also the new shear stress distribution at the centre line. This latter, and the values of u at $x = 0$, will be unchanged by any subsequent analysis, and so in a practical example these curves should be examined to ensure that they are satisfactory before proceeding further.

Due to the combination of engineers' theory and the exponential stress systems, errors additional to those quoted above are introduced into the displacement terms. In particular, at $x = 0$,

(1) $\frac{\partial}{\partial x}(u_w - u_b) \neq 0,$

(2) $\frac{\partial^2}{\partial x^2}(v_w - v_b) \neq 0,$

and at $x = l$

(3) $u_w - u_b \neq 0,$

(4) $v_w - v_b \neq 0.$

We may remove these errors by means of stress systems of the harmonic type, since because of their symmetry in x these systems will not alter the functions that we have previously

corrected in equations (34) to (39). Three harmonic stress systems are used ($m = 1, 3$ and 5) defined by (Γ_1, Λ_1), (Γ_3, Λ_3) and (Γ_5, Λ_5), the additional two variables being used to satisfy the conditions that the web shear at $x = l$, $y = h$ should have its engineers' theory value and that the boom shear at $x = 0$ should be zero.† The appropriate equations are as follows:

$$\sum_{1,3,5} \Lambda(-1)^{\frac{1}{2}(m+1)} = 0, \tag{40}$$

$$\sum_{1,3,5} \frac{\Gamma}{\beta}(-1)^{\frac{1}{2}(m+1)} = 0, \tag{41}$$

$$\{E(v_w - v_b)_{x=l}\}_{\text{eng.+exp.}} - \sum_{1,3,5} \frac{1}{\beta(\sinh\beta h \cosh\beta h - \beta h)} [\Gamma\{2\cosh^2\beta h\} + \Lambda\{\beta h + \sinh\beta h \cosh\beta h + \nu(\beta h - \sinh\beta h \cosh\beta h)\}] - \sum_{1,3,5} \frac{t_w}{\beta^4 I_b}\{\Gamma - \Lambda\beta a\} - \frac{t_w l^3}{I_b 3} \sum_{1,3,5} \frac{\Gamma}{\beta}(-1)^{\frac{1}{2}(m+1)} = 0, \tag{42}$$

$$\{E(u_w - u_b)_{x=l}\}_{\text{exp.}} - \sum_{1,3,5} \frac{(-1)^{\frac{1}{2}(m+1)}}{\beta(\sinh\beta h \cosh\beta h - \beta h)} \times [\Gamma\{\beta h + \sinh\beta h \cosh\beta h + \nu(\beta h - \sinh\beta h \cosh\beta h)\} + \Lambda\{2\sinh^2\beta h\}] + \sum_{1,3,5} \frac{t_w}{\beta^3}\left[\frac{\Gamma a}{I_b} - \frac{\Lambda\beta}{I_b}\left\{1 + \frac{a^2 A_b}{I_b}\right\}\right](-1)^{\frac{1}{2}(m+1)} + \frac{a t_w l^2}{I_b 2} \sum_{1,3,5} \frac{\Gamma}{\beta}(-1)^{\frac{1}{2}(m+1)} = 0. \tag{43}$$

$$\left\{E\frac{\partial^2}{\partial x^2}(v_w - v_b)_{x=0}\right\}_{\text{exp.}} - \sum_{1,3,5} \frac{\beta}{(\sinh\beta h \cosh\beta h - \beta h)} \times [\Gamma\{2\cosh^2\beta h\} + \Lambda\{\beta h + \sinh\beta h \cosh\beta h + \nu(\beta h - \sinh\beta h \cosh\beta h)\}] - \sum_{1,3,5} \frac{t_w}{\beta^2 I_b}\{\Gamma - \Lambda\beta a\} - \frac{t_w l}{I_b} \sum_{1,3,5} \frac{\Gamma}{\beta}(-1)^{\frac{1}{2}(m+1)} = 0, \tag{44}$$

$$\left\{E\frac{\partial}{\partial x}(u_w - u_b)_{x=0}\right\}_{\text{exp.}} + \sum_{1,3,5} \frac{1}{(\sinh\beta h \cosh\beta h - \beta h)} \times [\Gamma\{\beta h + \sinh\beta h \cosh\beta h + \nu(\beta h - \sinh\beta h \cosh\beta h)\} + \Lambda\{2\sinh^2\beta h\}] - \sum_{1,3,5} \frac{t_w}{\beta^2}\left[\frac{\Gamma a}{I_b} - \frac{\Lambda\beta}{A_b}\left\{1 + \frac{a^2 A_b}{I_b}\right\}\right] - \frac{a t_w l}{I_b} \sum_{1,3,5} \frac{\Gamma}{\beta}(-1)^{\frac{1}{2}(m+1)} = 0. \tag{45}$$

In virtue of equation (41), the last term in each of equations (42) to (45) is zero, and the solution is most readily obtained by substituting (40) and (41) in (42) to (45) and then solving the ensuing four simultaneous equations. Having determined (Γ_1, Λ_1), (Γ_3, Λ_3) and (Γ_5, Λ_5) we may then evaluate the displacements due to the harmonic terms.

The final displacements obtained by the addition of those due to engineers' theory, the exponential stress systems and the harmonic stress systems satisfy the following con-

† We are apparently wasting a variable here, since $S_b = 0$ at $x = 0$ has already been used as a condition for the exponential systems and in theory it is only necessary to make $S_b = 0$ at $x = 0$ for the two systems combined. In practice, however, the analysis has been found to give much better results when the condition is applied to each set of systems independently.

ditions, which are not all independent. Those asterisked are conditions which the stress distribution of the elementary theory of bending does not succeed in satisfying:

$$(1) \qquad u_w = u_b = 0 \qquad \text{at } x = 0,$$

$$(2) \qquad \frac{\partial u_w}{\partial x} = \frac{\partial u_b}{\partial x} \qquad \text{at } x = 0,$$

$$(3) \qquad \frac{\partial^2 u_w}{\partial x^2} = \frac{\partial^2 u_b}{\partial x^2} \overset{*}{=} 0 \qquad \text{at } x = 0,$$

$$(4) \qquad u_w = u_b \qquad \text{at } x = l,$$

$$(5) \qquad v_w = v_b \qquad \text{at } x = 0,$$

$$(6) \qquad \frac{\partial v_w}{\partial x} \overset{*}{=} \frac{\partial v_b}{\partial x} = 0 \qquad \text{at } x = 0,$$

$$(7) \qquad \frac{\partial^2 v_w}{\partial x^2} = \frac{\partial^2 v_b}{\partial x^2} \qquad \text{at } x = 0,$$

$$(8) \qquad \frac{\partial^3 v_w}{\partial x^3} = \frac{\partial^3 v_b}{\partial x^3} \overset{*}{=} 0 \qquad \text{at } x = 0,$$

$$(9) \qquad v_w \overset{*}{=} v_b \qquad \text{at } x = l,$$

$$(10) \qquad \frac{\partial u}{\partial y} \overset{*}{=} 0 \qquad \text{at } x = 0,\ y = h,$$

$$(11) \qquad \int_0^h uy \, dy \overset{*}{=} 0 \qquad \text{at } x = 0.$$

Further, the stresses derived from these final displacements satisfy the following conditions:

(12) The fluxes between web and boom are everywhere in equilibrium, and the internal stresses are always in equilibrium with the overall applied shear and bending moment.

$$(13) \qquad \sigma_x = (\sigma_x)_{\text{eng.}} \qquad \text{at } x = l,$$

$$(14) \qquad \sigma_y = (\sigma_y)_{\text{eng.}} = 0 \qquad \text{at } x = l,\ y = h,$$

$$(15) \qquad \tau_{xy} \overset{*}{=} 0 \qquad \text{at } x = 0,\ y = h,$$

$$(16) \qquad \tau_{xy} = (\tau_{xy})_{\text{eng.}} \qquad \text{at } x = l,\ y = h,$$

$$(17) \qquad \int_0^h \tau_{xy} \, dy = \int_0^h (\tau_{xy})_{\text{eng.}} \, dy \qquad \text{at } x = l,$$

$$(18) \qquad S_b \overset{*}{=} 0 \qquad \text{at } x = 0,$$

$$(19) \qquad S_b = (S_b)_{\text{eng.}} \qquad \text{at } x = l.$$

We have previously investigated the distributions of u and τ_{xy} at $x = 0$. Similarly, in a practical case, we must now determine the values of u, v and τ_{xy} at $x = l$ to ensure that they do not differ appreciably from engineers' theory. As a final check on the accuracy of the calculation, u_w, u_b, v_w, v_b, $\partial u_w/\partial x$, $\partial u_b/\partial x$, $\partial^2 v_w/\partial x^2$ and $\partial^2 v_b/\partial x^2$ should be evaluated for the complete range of x. Provided the web and boom curves are in reasonably close agreement we may say that the imposed stress systems do, at least in an overall sense, compensate for the errors in engineers' theory.

As far as stress concentration is concerned, we shall generally be interested in the stresses in the outer fibres of the boom, obtained as

$$(\sigma_x)_H = E\left\{\frac{\partial u_b}{\partial x} - (a+b)\frac{\partial^2 v_b}{\partial x^2}\right\}_{\mathrm{sss}} + (\sigma_x)_{H\,\mathrm{eng.}}, \tag{46}$$

where sss is a suffix denoting the superimposed stress systems. The stress concentration factor Ψ is then given by

$$\Psi = \frac{(\sigma_x)_H}{(\sigma_x)_{H\,\mathrm{eng.}}} = 1 + \frac{E\left\{\frac{\partial u_b}{\partial x} - (a+b)\frac{\partial^2 v_b}{\partial x^2}\right\}_{\mathrm{sss}}}{(\sigma_x)_{H\,\mathrm{eng.}}}. \tag{47}$$

4. A numerical example

As a practical example to which we may apply the above analysis we consider the beam shown in figure 2. This represents an undercarriage girder for a large aircraft, and it has been designed on the assumption that the material is light alloy having a permissible working stress of 15 tons/in.^{2} and a Poisson's ratio of 0·3.

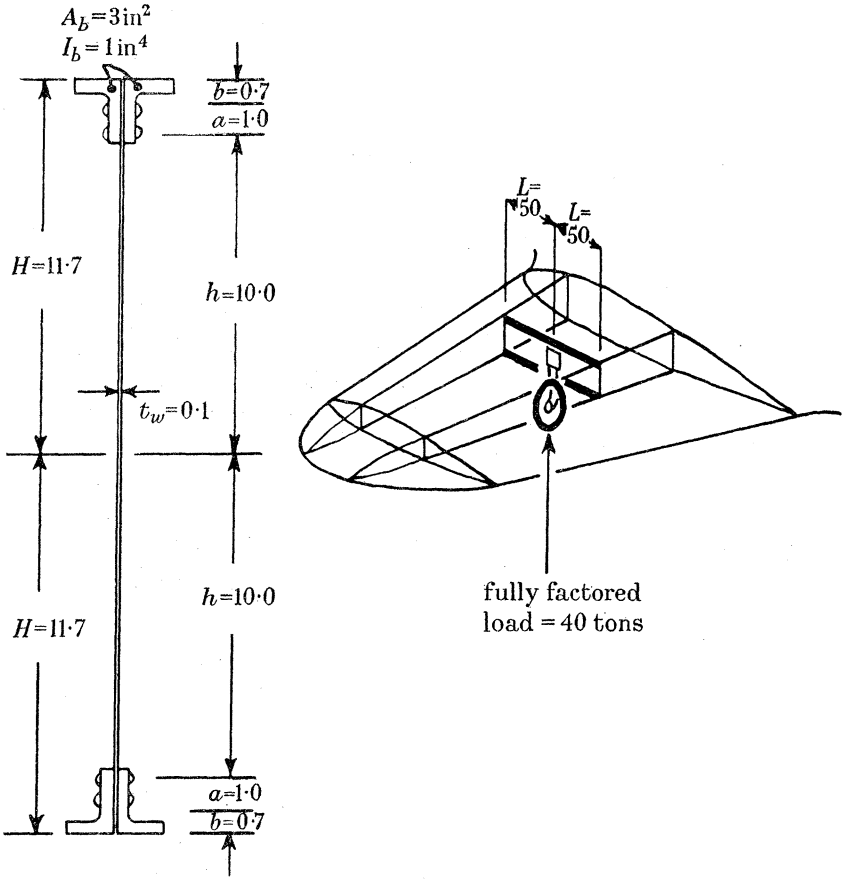

Figure 2. Undercarriage girder.

As a first measure we must determine the exponential coefficients (T_1), (T_2, U_2), (T_3) and (T_4, U_4) from equations (34) to (39). All the quantities are known except the length of beam considered, l. The choice of l is a matter of experience. In the present example three

preliminary calculations were made, using a simplified analysis, for values of l of $\frac{1}{2}h$, h and $\frac{3}{2}h$ (5, 10 and 15 in.), it being eventually decided from comparisons of the web and boom displacement curves at their junction that the last was the most satisfactory. It would seem that l must be sufficiently large so that the exponential terms can die away satisfactorily, without being so large as to make the analysis insensitive. The value is not at all critical, changes in l of as much as 50 % producing only small variations in the stress distribution.

The values of the coefficients obtained are as follows:

$$\left.\begin{aligned} T_1 &= -0{\cdot}084S, \\ T_2 &= -0{\cdot}577S, \\ T_3 &= -0{\cdot}051S, \\ T_4 &= -0{\cdot}161S, \\ U_2 &= 2{\cdot}42S, \\ U_4 &= -0{\cdot}01S. \end{aligned}\right\} \tag{48}$$

The distributions of τ_{xy} and u at $x = 0$ which are derived from these values are compared with the original engineers' theory distributions in figures 3 and 4. The associated displacements, slopes and curvatures are obtained as

$$x = 0: \quad \left.\begin{aligned} E\frac{\partial u_w}{\partial x} &= 0{\cdot}031S, \\ E\frac{\partial u_b}{\partial x} &= 0{\cdot}136S, \\ E\frac{\partial^2 v_w}{\partial x^2} &= -0{\cdot}338S, \\ E\frac{\partial^2 v_b}{\partial x^2} &= 0{\cdot}149S; \end{aligned}\right\} \tag{49}$$

$$x = l: \quad \left.\begin{aligned} Eu_w &= 0{\cdot}222S, \\ Eu_b &= 0{\cdot}870S, \\ Ev_w &= -14{\cdot}92S, \\ Ev_b &= 9{\cdot}46S. \end{aligned}\right\} \tag{50}$$

We must next solve for the harmonic terms, and on substituting equations (49) and (50) in (40) to (45) we obtain

$$\left.\begin{aligned} \Lambda_1 - \Lambda_3 + \Lambda_5 &= 0, \\ \Gamma_1 - \tfrac{1}{3}\Gamma_3 + \tfrac{1}{5}\Gamma_5 &= 0, \\ -884{\cdot}5\,\Gamma_1 - 16{\cdot}82\,\Gamma_3 - 5{\cdot}16\,\Gamma_5 + 59{\cdot}5\,\Lambda_1 + 0{\cdot}85\,\Lambda_3 + 0{\cdot}124\Lambda_5 - 24{\cdot}38S &= 0, \\ -59{\cdot}5\,\Gamma_1 + 0{\cdot}85\,\Gamma_3 - 0{\cdot}124\,\Gamma_5 + 43{\cdot}5\,\Lambda_1 - 7{\cdot}84\,\Lambda_3 + 4{\cdot}32\,\Lambda_5 - 0{\cdot}648S &= 0, \\ -9{\cdot}68\Gamma_1 - 1{\cdot}66\,\Gamma_3 - 1{\cdot}41\,\Gamma_5 + 0{\cdot}651\Lambda_1 + 0{\cdot}084\Lambda_3 + 0{\cdot}034\Lambda_5 - 0{\cdot}487S &= 0, \\ -6{\cdot}23\Gamma_1 - 0{\cdot}267\Gamma_3 - 0{\cdot}0649\Gamma_5 + 4{\cdot}56\,\Lambda_1 + 2{\cdot}46\,\Lambda_3 + 2{\cdot}26\,\Lambda_5 - 0{\cdot}0105S &= 0, \end{aligned}\right\} \tag{51}$$

whence

$$\left.\begin{aligned}\Gamma_1 &= -0{\cdot}0268S,\\ \Gamma_3 &= -0{\cdot}1076S,\\ \Gamma_5 &= -0{\cdot}0454S,\\ \Lambda_1 &= -0{\cdot}0227S,\\ \Lambda_3 &= -0{\cdot}0088S,\\ \Lambda_5 &= \ \ 0{\cdot}0139S.\end{aligned}\right\} \tag{52}$$

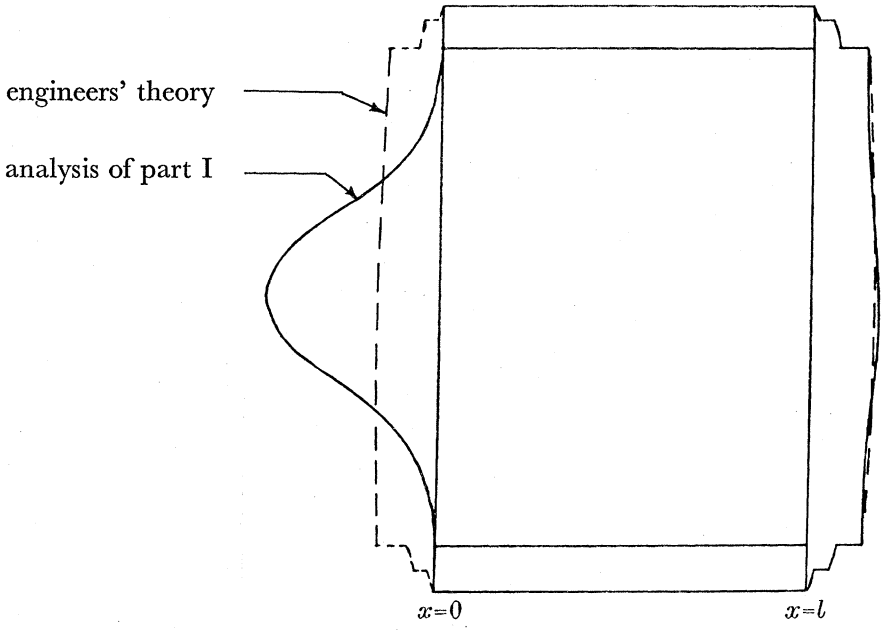

FIGURE 3. Distributions of τ_{xy}.

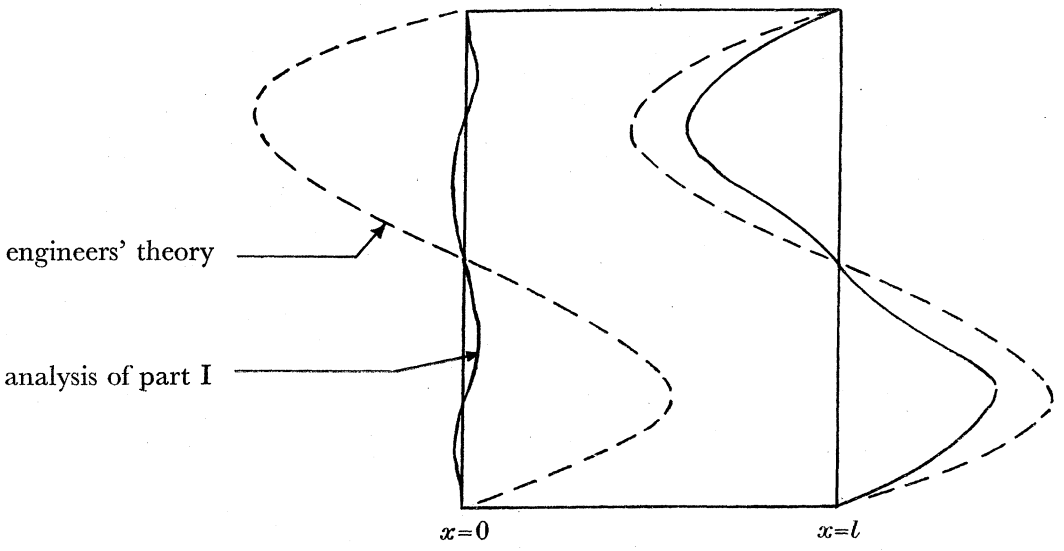

FIGURE 4. Distributions of u_{web}.

We are now in a position to undertake the checks mentioned at the end of § 3. The distributions of τ_{xy} and u at $x = l$ are shown compared with those at $x = 0$ in figures 3 and 4. It will be seen that we have succeeded in obtaining satisfactory centre-line distributions without appreciably affecting the values at $x = l$. The distribution of v must also be sensibly that of engineers' theory, since (as will be seen from later curves) the rate of change of shear is small at $x = l$. As a further point it should be remembered that any corrections to the final stress distribution which might be necessary due to the remaining small incompatibilities at $x = l$ would be a maximum at this section, and that their effect at $x = 0$, the section at which we shall be most interested in the stresses, would be quite negligible.

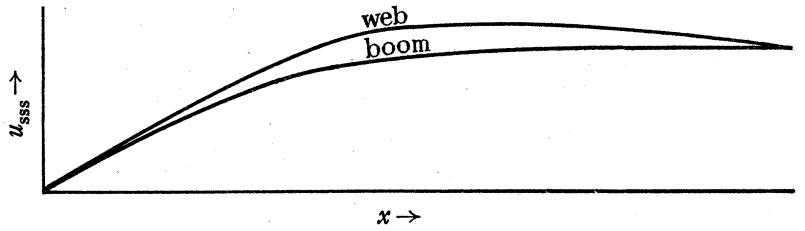

FIGURE 5. Comparison of u_w and u_b.

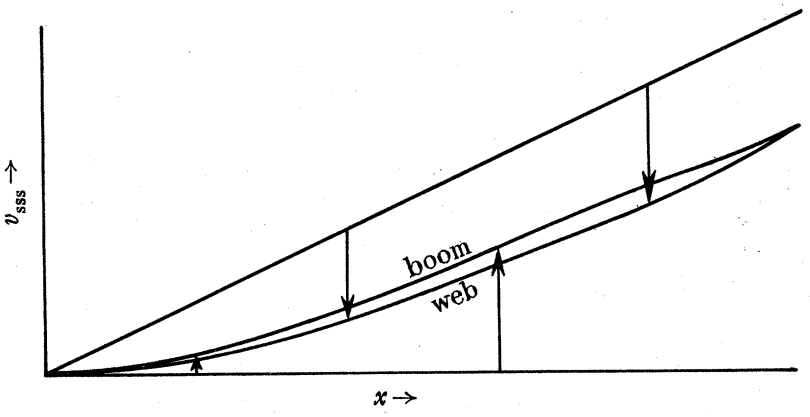

FIGURE 6. Comparison of v_w and v_b.

The final values of u_w, u_b, v_w, v_b, $\partial u_w/\partial x$, $\partial u_b/\partial x$, $\partial^2 v_w/\partial x^2$ and $\partial^2 v_b/\partial x^2$ are plotted in figures 5 to 8. It should be noted that these are the curves for the displacements due to the superimposed stress systems only, and therefore discrepancies between them are second-order effects as far as final overall stresses are concerned. The curves of v_w and v_b are shown closing the engineers' theory gap of equation (5); as with the other functions, the displacements of the elementary theory, $v = -\int_0^x \int_0^x (M/EI)\,dx\,dx$ in this case, must be added to obtain overall values. It will be seen that the agreement between the curves for web and boom is sufficiently close for the values of the boom outer-fibre stress due to the imposed stress systems, plotted in figure 9, to be treated with confidence. The stress-concentration factor at the origin is obtained as

$$\Psi = 1 + 0{\cdot}90\frac{h}{L}. \tag{53}$$

For the particular case of the undercarriage girder, $L/h = 5$, and $\Psi = 1{\cdot}18$, the outer-fibre stress being 17·4 tons/in.^{2} compared with 14·7 tons/in.^{2} according to engineers' theory.

The girder would have an actual reserve factor of 0·86, compared with an apparent one of 1·02.

The total boom outer-fibre stress is plotted in figure 10, where it is compared with the engineers' theory distribution. It will be noticed that our present analysis gives a stress concentration which is distributed over several inches of the beam, i.e. the concentration is not of the 'point maximum' type which can be relieved by a very localized yielding of the material.

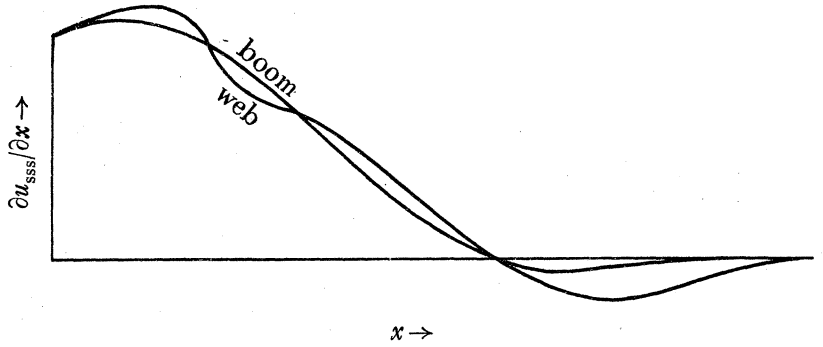

FIGURE 7. Comparison of $\partial u_w/\partial x$ and $\partial u_b/\partial x$.

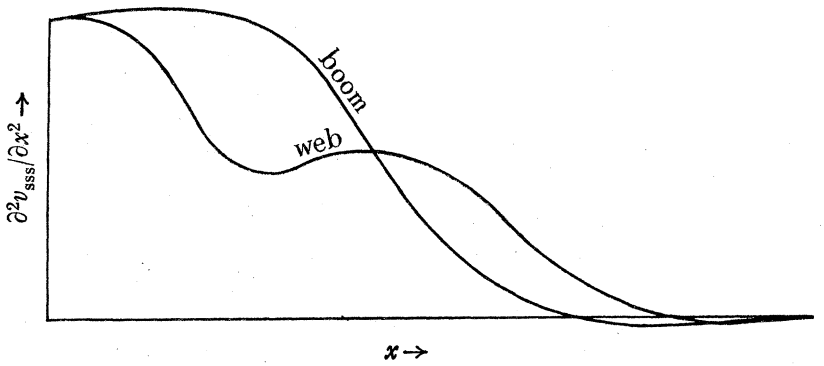

FIGURE 8. Comparison of $\partial^2 v_w/\partial x^2$ and $\partial^2 v_b/\partial x^2$.

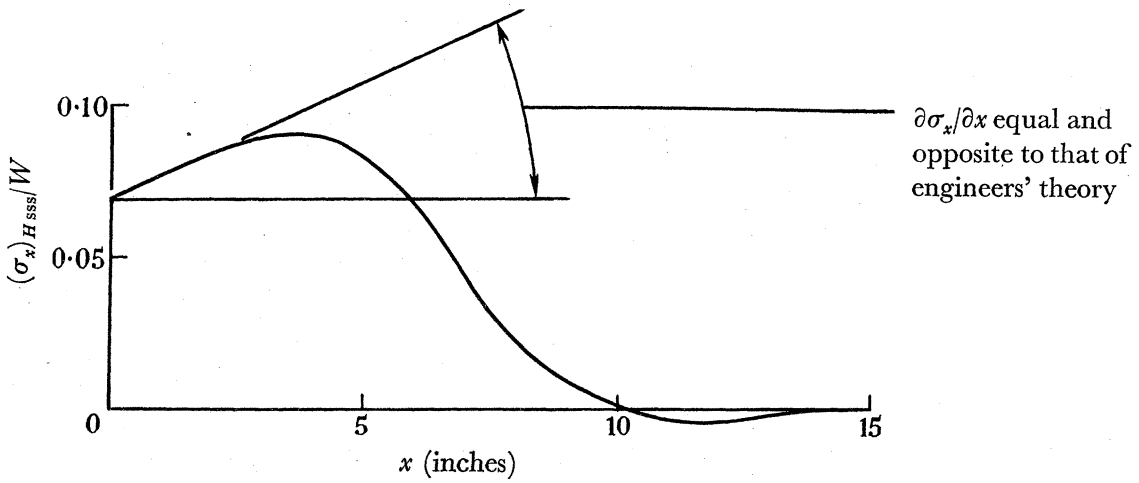

FIGURE 9. Outer fibre stress due to superimposed stress systems.

Figures 11 and 12 show the cross-tensile and shear fluxes between the boom and the web, the area under the former curve being, of course, equal to $-2S_{b\,\mathrm{eng.}}$. The general shapes of the curves conform with what might be expected from simple physical considerations.

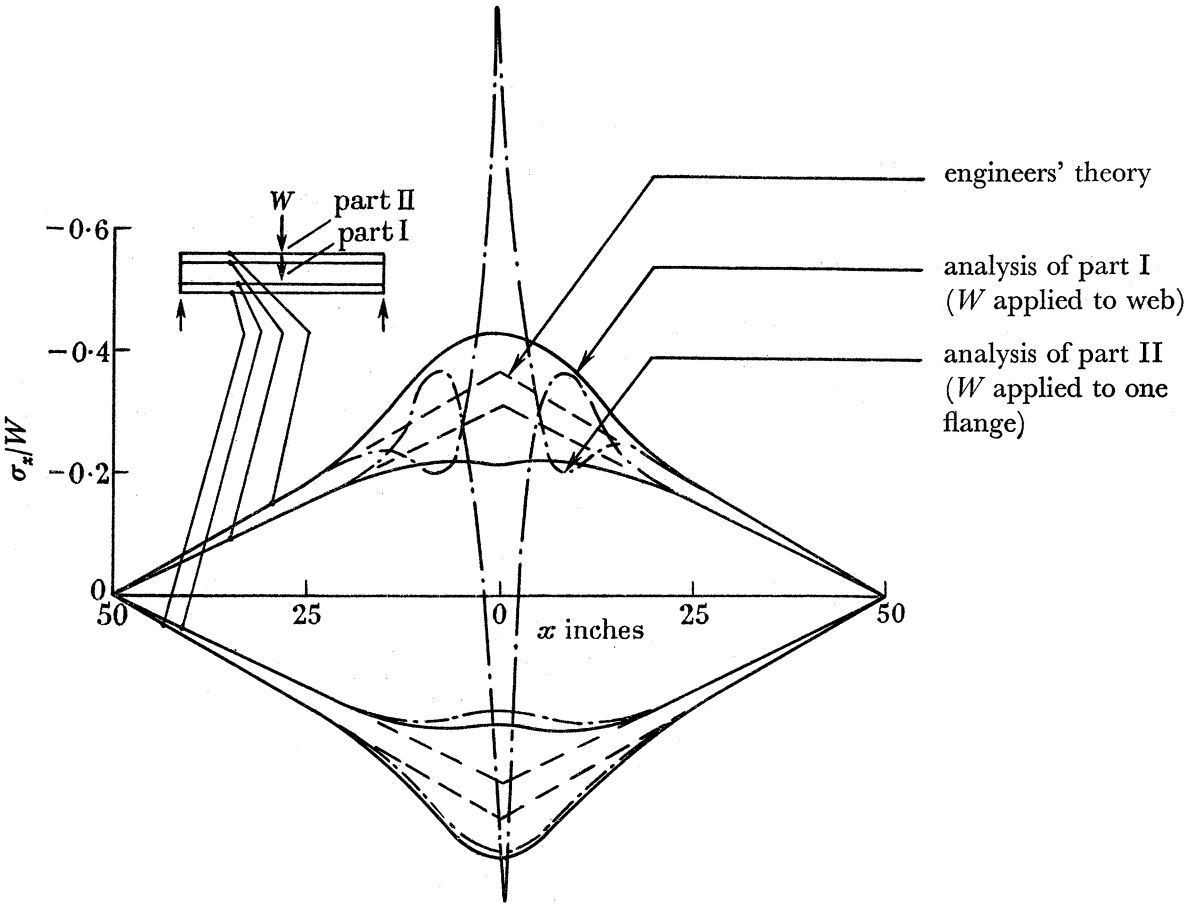

FIGURE 10. Total fibre stresses.

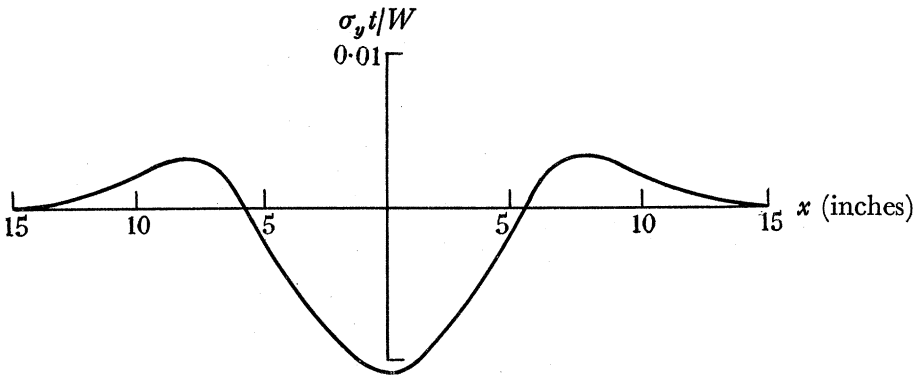

FIGURE 11. Cross-tensile flux between web and boom.

Figure 13 shows the final distribution of σ_x at the loading section and compares this with the distribution according to engineers' theory. It will be seen that the maximum variation from engineers' theory occurs in the web at $y = h$, although this is, fortunately, in the sense of reducing the overall stress.

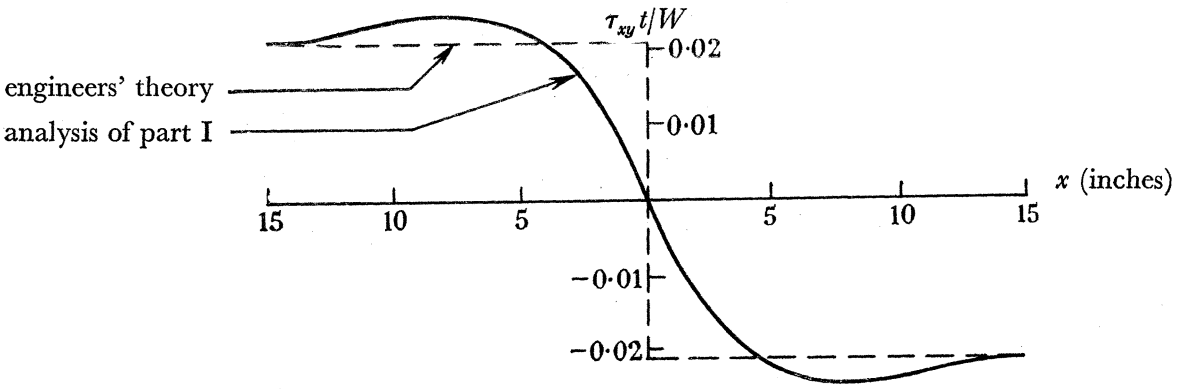

FIGURE 12. Shear flux between web and boom.

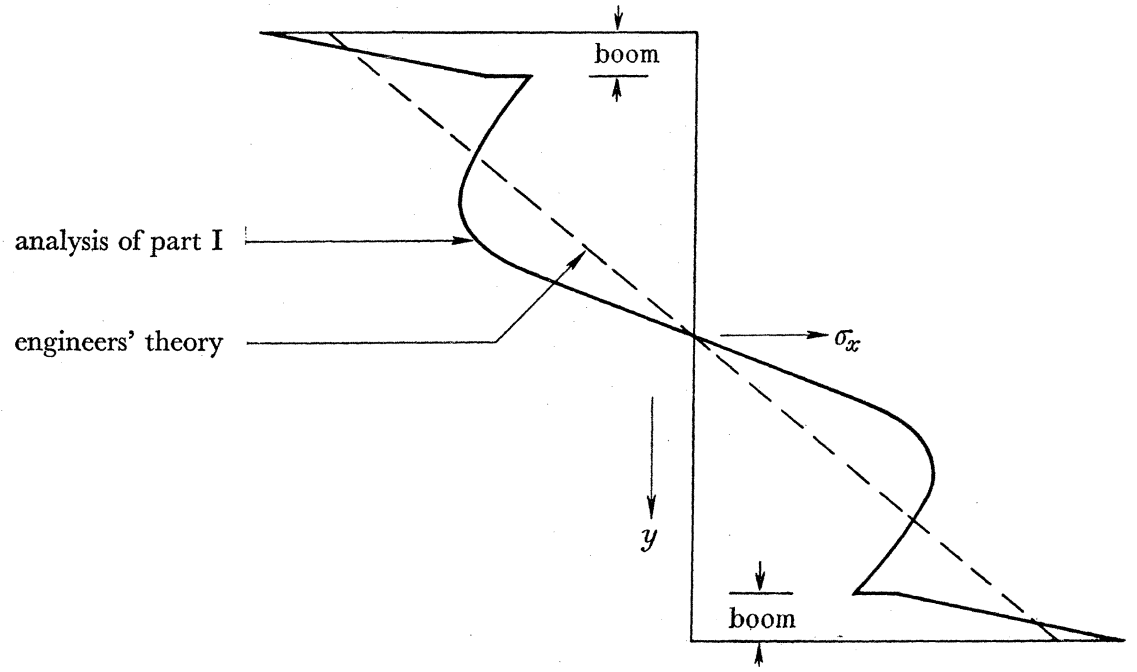

FIGURE 13. Direct stresses at the loading section.

5. GENERAL CONSIDERATIONS

The problem of the stress distribution in a uniform flanged beam effectively depends, apart from simple multiple relationships, on four parameters:

$$\nu, \quad \frac{a}{h}, \quad \frac{A_b}{ht_w}, \quad \frac{I_b}{h^3t_w}. \tag{54}$$

In the present paper it will be assumed that $\nu = 0{\cdot}3$, the usual value for steels and light alloys, so that we are left with three parameters for investigation. Study of standard section tables and examples from aircraft design suggested that the range of these parameters which is of practical interest was as follows:

$$\left.\begin{aligned} 0 \leqslant \frac{a}{h} \leqslant 0{\cdot}1, \\ 1 \leqslant \frac{A_b}{ht_w} \leqslant 9, \\ 0{\cdot}003 \leqslant \frac{I_b}{h^3t_w} \leqslant 0{\cdot}03. \end{aligned}\right\} \tag{55}$$

Accordingly in the derivation of general curves a 'central' point (0·05, 3, 0·01) was first taken and the stress concentration in the outer fibre of the boom at the loading section was calculated. It was found most convenient to express this in terms of two non-dimensional functions f and g, where

$$(\sigma_x)_H = (\sigma_x)_{H\,\text{eng.}} + \frac{W}{2ht_w}\left[f\left\{\frac{a}{h}, \frac{A_b}{ht_w}, \frac{I_b}{h^3t_w}\right\} - \frac{(a+b)}{h}\,g\left\{\frac{a}{h}, \frac{A_b}{ht_w}, \frac{I_b}{h^3t_w}\right\}\right]. \tag{56}$$

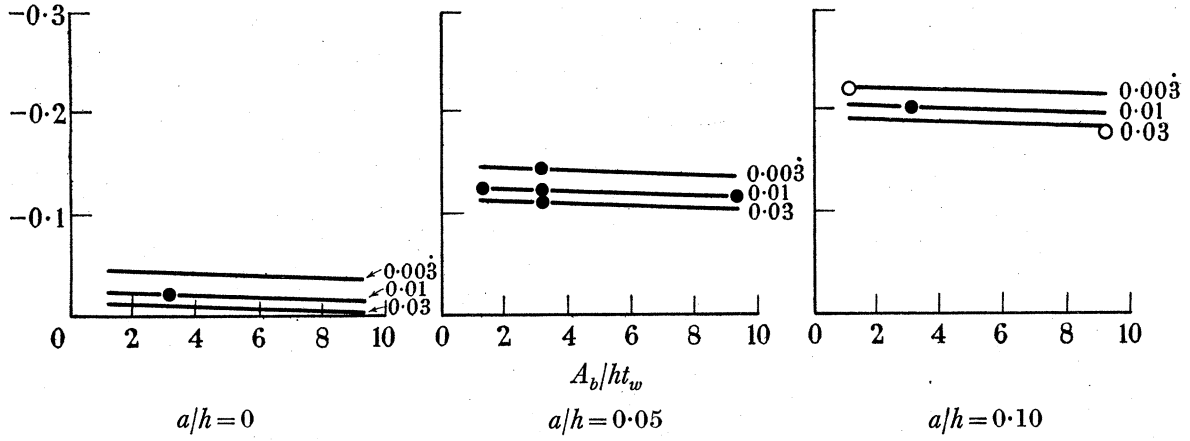

FIGURE 14. Function f. Values of I_b/h^3t_w are given against the curves.
●, basic calculations; ○, check calculations.

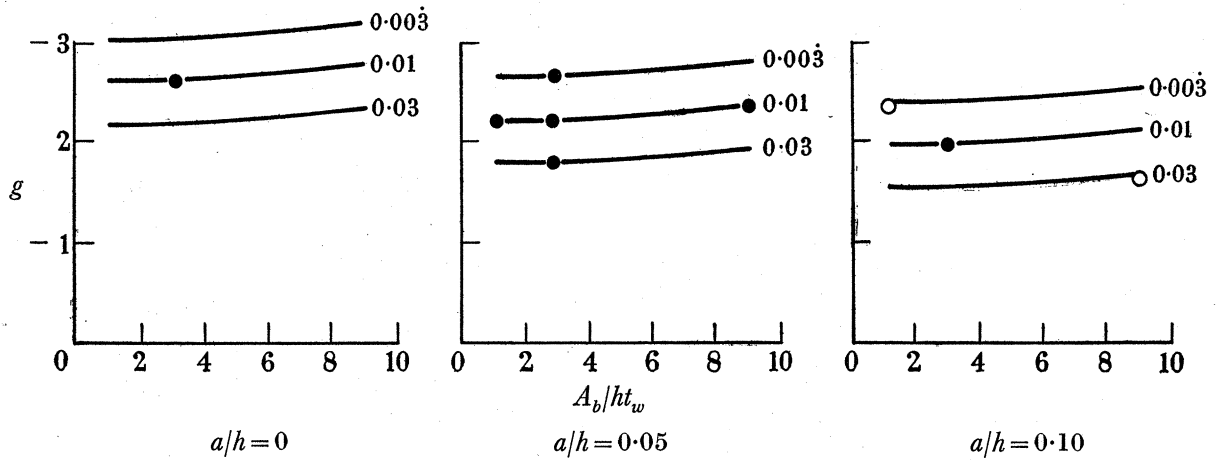

FIGURE 15. Function g. Values of I_b/h^3t_w are given against the curves.
●, basic calculations; ○, check calculations.

Starting from this central point, each parameter was varied in turn to the extremes of its range until altogether seven sets of values of f and g had been obtained. General curves were then calculated on the assumption that $\partial f/\partial(a/h)$ was a function of a/h only and similarly for g and the other parameters. As a check on the validity of this assumption two further calculations were made for the points (0·10, 1, 0·00$\dot{3}$) and (0·10, 9, 0·03). It was found that the values of f and g predicted by the general curves and those obtained by direct calculation were in close agreement.* The general curves of f and g are given in figures 14 and 15, and

* By extrapolation to $I_b=0$, our curves are also found to be in good agreement with the solution obtained for this case by Hildebrand & Reissner (1942).

the outer-fibre stress at a loading section in any uniform flanged beam may be calculated from them by means of equation (56).

On studying the curves in detail, three relationships become apparent: g is practically independent of a/h and A_b/ht_w; and $(f-ag/h)$ is generally small compared with bg/h, as would be expected, since one represents the stress due to end-load and the other that due to bending. Accordingly it follows that

$$(\sigma_x)_H = (\sigma_x)_{H\,\text{eng.}} - \frac{W_b}{2h^2t_w}\,g\left\{\frac{I_b}{h^3t_w}\right\}, \tag{57}$$

and on plotting the log-log curves of the various parameters, we find that this relationship may be very closely expressed over the whole of the range considered by

$$(\sigma_x)_H = (\sigma_x)_{H\,\text{eng.}} + 0{\cdot}3\,\frac{Wb}{h^2t_w}\sqrt[4]{\frac{h^3t_w}{I_b}} \tag{58}$$

or

$$\Psi = 1 + \frac{0{\cdot}3\,\dfrac{Wb}{h^2t_w}\sqrt[4]{\dfrac{h^3t_w}{I_b}}}{(\sigma_x)_{H\,\text{eng.}}}. \tag{59}$$

If we assume the beam to be simply supported on a semi-span L and centrally loaded,

$$\Psi \backsimeq 1 + 1{\cdot}2L^{-1}h^{-\frac{1}{2}}bA_bI_b^{-\frac{1}{4}}t_w^{-\frac{3}{4}}, \tag{60}*$$

so that the maximum departures from engineers' theory will occur in short beams having large booms and thin webs—conclusions which might be expected from physical considerations.

PART II. BEAM LOADED THROUGH THE FLANGES

6. Equal and opposite loads on the flanges

6·1. *Introduction*

In part I we have considered the problem of the stress distribution in a flanged beam loaded by means of a patch plate attached to the web. We turn now to beams in which load is applied to one or both flanges.

Any case of flange loading can be considered as the sum of a symmetric system in which two loads equal in magnitude and opposite in direction are applied to the two flanges and an asymmetric system in which the loads have the same direction. We shall for the moment restrict our investigation to the symmetric system.

An approximate solution similar to that used in part I can be developed, but because of the condition of zero shear in the web at the loading section it is possible to solve the problem exactly.† We begin by considering the comparatively easy case of a flange resting on a semi-infinite plate and then go on to develop the full analysis for a beam of finite depth. It is shown that for most practical cases the simpler analysis is sufficiently accurate, and we proceed to investigate the effects of the various parameters and to develop a formula for the stress in the outer fibres of the flanges at the loading section.

* The approximation is that a/h, b/h and I_b/A_bh^2 are negligible compared with unity.
† Our analysis is basically a development of that of Filon (1903).

6·2. *Flange resting on a semi-infinite plate*

Consider the flange shown in figure 16, subjected to a normal loading $q(x)$ per unit length and resting on a semi-infinite plate of thickness t_w. Then if the end load, shear and bending moment in the flange are P_b, S_b and M_b, and the edge stresses in the plate are σ_y and τ_{xy}, we have for the equilibrium of an element of flange (figure 17)

$$\left.\begin{aligned} \frac{\partial P_b}{\partial x} &= -t_w \tau_{xy}, \\ \frac{\partial S_b}{\partial x} &= q(x) - t_w \sigma_y, \\ \frac{\partial M_b}{\partial x} &= S_b - a\tau_{xy}. \end{aligned}\right\} \tag{61}$$

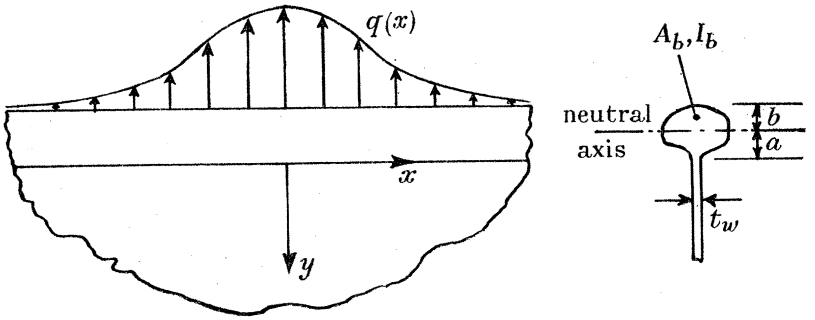

FIGURE 16. Flange on semi-infinite plate.

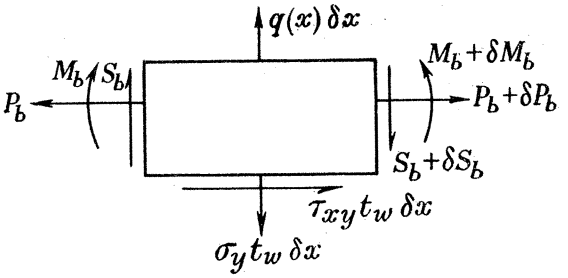

FIGURE 17. Equilibrium of an element of flange.

Denoting the displacements in the directions of x and y at $y = 0$ by u and v,

$$\left.\begin{aligned} \frac{\partial u}{\partial x} &= \frac{P_b}{A_b E} + \frac{M_b a}{I_b E}, \\ \frac{\partial^2 v}{\partial x^2} &= -\frac{M_b}{I_b E}. \end{aligned}\right\} \tag{62}$$

From equations (61) and (62),

$$\left.\begin{aligned} t_w \tau_{xy} &= -A_b E \left\{\frac{\partial^2 u}{\partial x^2} + a\frac{\partial^3 v}{\partial x^3}\right\}, \\ t_w \sigma_y - q(x) &= (I_b + a^2 A_b) E \frac{\partial^4 v}{\partial x^4} + a A_b E \frac{\partial^3 u}{\partial x^3}. \end{aligned}\right\} \tag{63}$$

Now let us apply the stress function

$$\phi = (C+Dy)\,\mathrm{e}^{-\alpha y}\cos\alpha x \tag{64}$$

to the plate. The stresses are given by

$$\left.\begin{aligned}\sigma_x &= \{-2D\alpha+\alpha^2(C+Dy)\}\,\mathrm{e}^{-\alpha y}\cos\alpha x,\\ \sigma_y &= -\alpha^2(C+Dy)\,\mathrm{e}^{-\alpha y}\cos\alpha x,\\ \tau_{xy} &= \alpha\{D-\alpha(C+Dy)\}\,\mathrm{e}^{-\alpha y}\sin\alpha x,\end{aligned}\right\} \tag{65}$$

and the displacements by

$$\left.\begin{aligned}Eu &= \{(1+\nu)\,\alpha(C+Dy)-2D\}\,\mathrm{e}^{-\alpha y}\sin\alpha x,\\ Ev &= \{(1+\nu)\,\alpha(C+Dy)+D(1-\nu)\}\,\mathrm{e}^{-\alpha y}\cos\alpha x-\{(1+\nu)\,\alpha C+D(1-\nu)\},\end{aligned}\right\} \tag{66}$$

using the rigid-body conditions $u = v = \partial v/\partial x = 0$ at the origin.

At $y = 0$

$$\left.\begin{aligned}\sigma_y &= -\alpha^2 C\cos\alpha x,\\ \tau_{xy} &= \alpha(D-\alpha C)\sin\alpha x,\\ Eu &= \{(1+\nu)\,\alpha C-2D\}\sin\alpha x,\\ Ev &= \{(1+\nu)\,\alpha C+D(1-\nu)\}\,(\cos\alpha x-1).\end{aligned}\right\} \tag{67}$$

On substituting (67) in (63) and putting $q(x) = \cos\alpha x$, we find

$$\left.\begin{aligned}C &= -\frac{t_w+2\alpha A_b+\alpha^2(1-\nu)\,A_b a}{\alpha^2 t_w^2+2\alpha^3 A_b t_w+2(1-\nu)\,\alpha^4 a A_b t_w+2\alpha^5(I_b+a^2A_b)\,t_w+\alpha^6(1+\nu)\,(3-\nu)\,A_b I_b},\\ D &= -\alpha\left\{\frac{t_w+\alpha(1+\nu)\,A_b-\alpha^2(1+\nu)\,A_b a}{\alpha^2 t_w^2+2\alpha^3 A_b t_w+2(1-\nu)\,\alpha^4 a A_b t_w+2\alpha^5(I_b+a^2A_b)\,t_w+\alpha^6(1+\nu)\,(3-\nu)\,A_b I_b}\right\}.\end{aligned}\right\} \tag{68}$$

Now by Fourier's integral theorem, any even system of loading $q(x)$ can be put in the form

$$\begin{aligned}q(x) &= \frac{2}{\pi}\int_0^\infty \mathrm{d}\alpha\int_0^\infty q(\chi)\cos\chi\alpha\cos\alpha x\,\mathrm{d}\chi\\ &= \int_0^\infty F(\alpha)\cos\alpha x\,\mathrm{d}\alpha,\end{aligned} \tag{69}$$

where

$$F(\alpha) = \frac{2}{\pi}\int_0^\infty q(\chi)\cos\chi\alpha\,\mathrm{d}\chi. \tag{70}$$

Let us suppose $q(x)$ to be constant at $\frac{1}{2}Q$ between $x = \pm 1/Q$. Then

$$\begin{aligned}F(\alpha) &= \frac{2}{\pi}\int_0^{1/Q}\frac{Q}{2}\cos\chi\alpha\,\mathrm{d}\chi\\ &= \frac{1}{\pi}\frac{Q}{\alpha}\sin\frac{\alpha}{Q},\end{aligned} \tag{71}$$

whence

$$q(x) = \int_0^\infty \frac{1}{\pi}\frac{Q}{\alpha}\sin\frac{\alpha}{Q}\cos\alpha x\,\mathrm{d}\alpha. \tag{72}$$

From equations (67), (68) and (72) the boundary stresses appropriate to this form of loading are given by

$$\left.\begin{aligned}\sigma_y &= \int_0^\infty \frac{Q\alpha}{\pi}\sin\frac{\alpha}{Q}\cos\alpha x\,\frac{t_w+2\alpha A_b+\alpha^2(1-\nu)\,aA_b}{\alpha^2t_w^2+2\alpha^3A_bt_w+2(1-\nu)\,\alpha^4aA_bt_w+2a^5(I_b+a^2A_b)\,t_w+\alpha^6(1+\nu)\,(3-\nu)\,A_bI_b}\,\mathrm{d}\alpha,\\ \tau_{xy} &= \int_0^\infty \frac{Q\alpha}{\pi}\sin\frac{\alpha}{Q}\sin\alpha x\,\frac{\alpha(1-\nu)\,A_b+2\alpha^2aA_b}{\alpha^2t_w^2+2\alpha^3A_bt_w+2(1-\nu)\,\alpha^4aA_bt_w+2a^5(I_b+a^2A_b)\,t_w+\alpha^6(1+\nu)\,(3-\nu)\,A_bI_b}\,\mathrm{d}\alpha.\end{aligned}\right\} \tag{73}$$

We consider first the particular case $a=0$, $A_b=\infty$, when

$$\sigma_y = \int_0^\infty \frac{Q}{\pi t}\sin\frac{\alpha}{Q}\cos\alpha x\,\frac{1}{\alpha\left\{1+\dfrac{(1+\nu)\,(3-\nu)}{2}\dfrac{I_b}{t_w}\alpha^3\right\}}\,\mathrm{d}\alpha. \tag{74}$$

For $Q=\infty$ (unit point load)

$$\begin{aligned}\sigma_y &= \int_0^\infty \frac{\cos\alpha x}{\pi t_w\left\{1+\dfrac{(1+\nu)\,(3-\nu)}{2}\dfrac{I_b}{t_w}\alpha^3\right\}}\,\mathrm{d}\alpha\\ &= \int_0^\infty \frac{\cos\eta x/J}{\pi J t_w}\frac{1}{1+\eta^3}\,\mathrm{d}\eta,\end{aligned} \tag{75}$$

where

$$\left.\begin{aligned}\eta &= J\alpha,\\ J^3 &= \frac{(1+\nu)\,(3-\nu)}{2}\frac{I_b}{t_w}.\end{aligned}\right\} \tag{76}$$

When $x=0$,

$$\sigma_y = \frac{2}{3\sqrt{3}\,Jt_w}; \tag{77}$$

the general curve is plotted in figure 18.

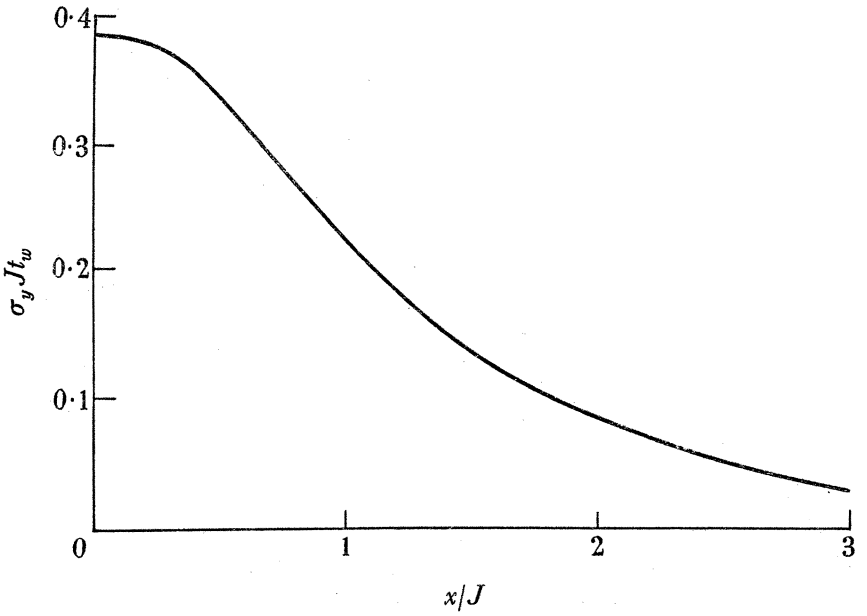

FIGURE 18. Transverse stress between flange and plate.

For finite values of Q, we have from equation (74)

$$\sigma_y = \int_0^\infty \frac{Q}{2\pi t_w}\left\{\sin\alpha\left(\frac{1}{Q}+x\right)+\sin\alpha\left(\frac{1}{Q}-x\right)\right\}\frac{1}{\alpha\left\{1+\frac{(1+\nu)(3-\nu)}{2}\frac{I_b}{t_w}\alpha^3\right\}}\,\mathrm{d}\alpha$$

$$= \int_0^\infty \frac{Q}{2\pi t_w}\frac{\sin\zeta}{\zeta}\left[\frac{1}{1+c^3\zeta^3}+\frac{1}{1+d^3\zeta^3}\right]\mathrm{d}\zeta \qquad (78)$$

for points inside the load, and

$$\int_0^\infty \frac{Q}{2\pi t_w}\frac{\sin\zeta}{\zeta}\left[\frac{1}{1+c^3\zeta^3}-\frac{1}{1+d\zeta^3}\right]\mathrm{d}\zeta \qquad (79)$$

for points outside the load, where

$$\left.\begin{aligned} c &= J\Big/\left(\frac{1}{Q}+x\right), \\ d &= \left|J\Big/\left(\frac{1}{Q}-x\right)\right|. \end{aligned}\right\} \qquad (80)$$

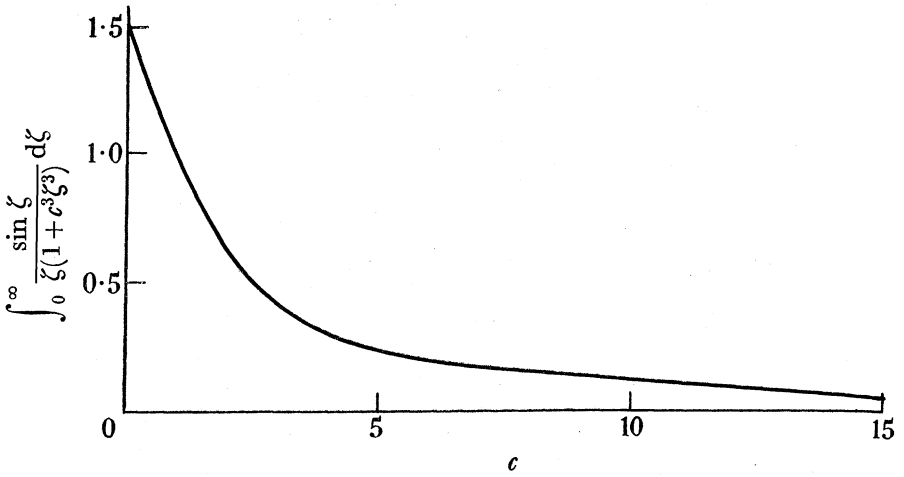

FIGURE 19. The function $\int_0^\infty \frac{\sin\zeta}{\zeta(1+c^3\zeta^3)}\mathrm{d}\zeta$.

The function $\int_0^\infty \frac{\sin\zeta}{\zeta(1+c^3\zeta^3)}\,\mathrm{d}\zeta$ is shown plotted in figure 19. From it σ_y for any value of x can be obtained. Figure 20 shows σ_y as a function of x for $Q = 1/2t_w$,* $\nu = 0{\cdot}3$, and various values of I_b. It will be seen that, as would be expected, increasing flange stiffness distributes the load farther over the plate. Figure 21 compares the value of σ_y at the origin for $Q = 1/2t_w$, with that for $Q = \infty$, for various I_b. Over the practical range the two are identical, and so we shall in future restrict our investigation to the case $Q = \infty$ (i.e. a point load).† It may be noted that equation (79) gives us an alternative method of calculating σ_y for $Q = \infty$, since in the limit it becomes

$$\sigma_y = \int_0^\infty \frac{3}{\pi t_w x}\sin\frac{x\eta}{J}\frac{\eta^2}{(1+\eta^3)^2}\,\mathrm{d}\eta. \qquad (81)$$

* I.e. with the load distributed over a distance equal to four times the web thickness.

† Experimental work by Hendry (1949) supports the analysis in suggesting that the load distribution is unimportant.

τ_{xy} for $a = 0$, $A_b = \infty$, $Q = \infty$ may be written from equation (73) as

$$\tau_{xy} = \int_0^\infty \frac{1-\nu}{2\pi t_w J} \sin\frac{\eta x}{J} \frac{1}{1+\eta^3} \mathrm{d}\eta. \tag{82}$$

It is plotted in figure 22.

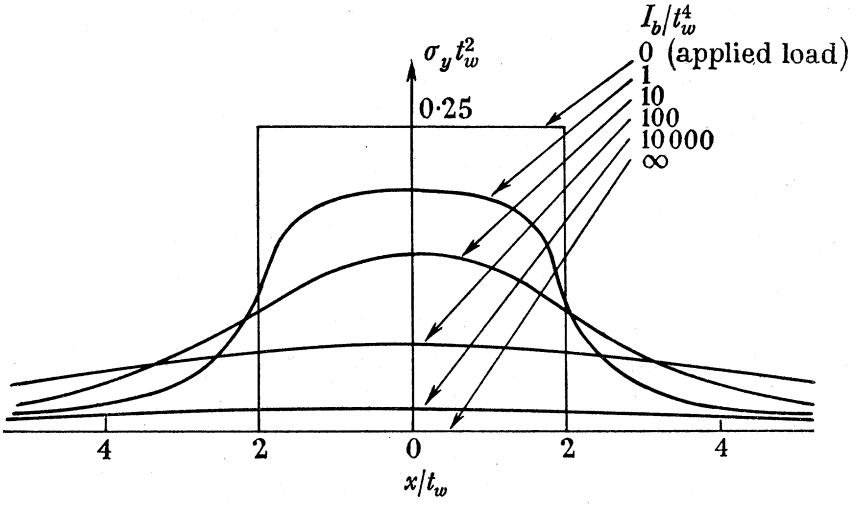

FIGURE 20. σ_y as a function of I_b. $Q = 1/2t_w$, $\nu = 0{\cdot}3$.

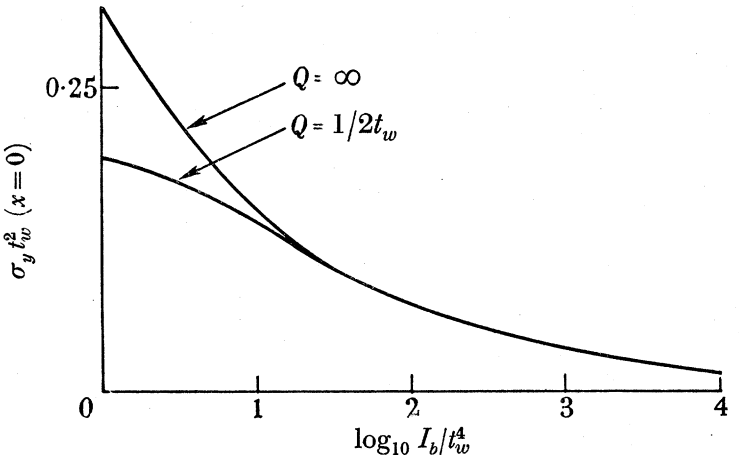

FIGURE 21. σ_y at the origin for $Q = 1/2t_w$ and ∞, $\nu = 0{\cdot}3$.

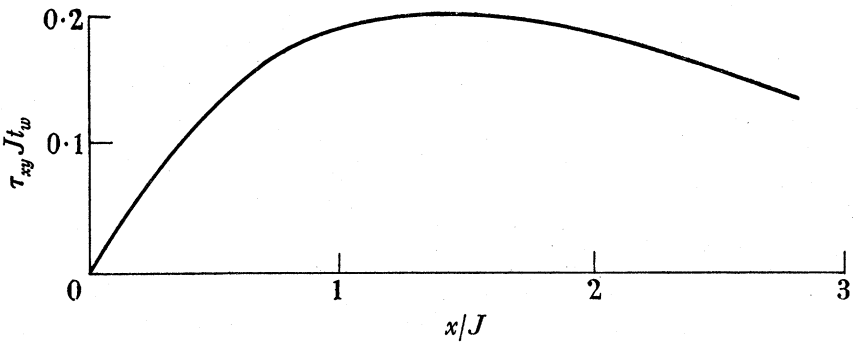

FIGURE 22. Shear stress between flange and plate.

The shear in the flange, S_b, is obtained by the integration of equation (75) as

$$S_b = -\int_0^\infty \frac{1}{\pi} \sin\frac{\eta x}{J} \frac{1}{\eta(1+\eta^3)}\,\mathrm{d}\eta + \tfrac{1}{2}. \tag{83}$$

This is plotted in figure 23, and by consideration of this curve it may be shown that the shear deformations of the flange, which we have ignored in our calculations, are in fact negligible.

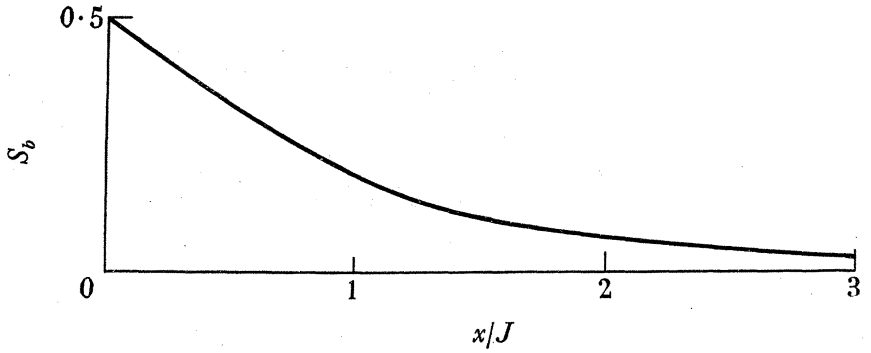

FIGURE 23. Shear in flange.

The bending moment in the flange must now be obtained. On integrating equation (83) we find

$$\begin{aligned} M_b - M_{b_0} &= -\int_0^\infty \frac{J}{\pi}\left(1-\cos\frac{x\eta}{J}\right)\frac{1}{\eta^2(1+\eta^3)}\,\mathrm{d}\eta + \frac{x}{2} \\ &= -\int_0^\infty \frac{J}{\pi}\left(1-\cos\frac{x\eta}{J}\right)\frac{1}{\eta^2}\,\mathrm{d}\eta + \int_0^\infty \frac{J}{\pi}\left(1-\cos\frac{x\eta}{J}\right)\frac{\eta}{1+\eta^3}\,\mathrm{d}\eta + \frac{x}{2}. \end{aligned} \tag{84}$$

Now the first and last terms in equation (84) cancel out, because

$$\begin{aligned} &\int_0^\infty \frac{J}{\pi}\left(1-\cos\frac{x\eta}{J}\right)\frac{1}{\eta^2}\,\mathrm{d}\eta \\ &\quad = \int_0^\infty \frac{x}{\pi}\frac{(1-\cos 2z)}{2z^2}\,\mathrm{d}z \\ &\quad = \int_0^\infty \frac{x}{\pi}\frac{\sin^2 z}{z^2}\,\mathrm{d}z \\ &\quad = \frac{x}{2}, \end{aligned}$$

whence

$$M_b - M_{b_0} = \int_0^\infty \frac{J}{\pi}\left(1-\cos\frac{x\eta}{J}\right)\frac{\eta}{1+\eta^3}\,\mathrm{d}\eta. \tag{85}$$

Now $M_b - M_{b_0}$ is finite throughout the range of integration, so that as x tends to infinity, the contribution to the integral of the rapidly varying function $(1-\cos x\eta/J)$ will tend to its mean value, i.e. unity. Thus, since $M_b = 0$ at $x = \infty$

$$\begin{aligned} M_{b_0} &= -\int_0^\infty \frac{J}{\pi}\frac{\eta}{1+\eta^3}\,\mathrm{d}\eta \\ &= -\frac{2J}{3\sqrt{3}}, \end{aligned} \tag{86}$$

and
$$M_b = \frac{x}{2} - \frac{2J}{3\sqrt{3}} - \int_0^\infty \frac{J}{\pi}\left(1-\cos\frac{x\eta}{J}\right)\frac{1}{\eta^2(1+\eta^3)}\,d\eta. \tag{87}$$

M_b is plotted as a function of x in figure 24.

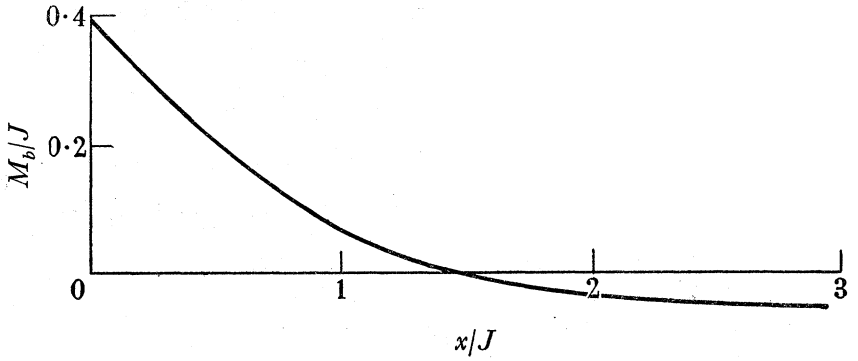

FIGURE 24. Bending moment in flange.

The stress in the outer fibre at the loading section may be obtained from equation (86) as

$$(\sigma_x)_H = \frac{2J}{3\sqrt{3}}\frac{b}{I_b}W, \quad \text{where } W \text{ is the applied load,}$$
$$= 0{\cdot}4644\frac{Wt_w b}{I_b}\sqrt[3]{\frac{I_b}{t_w^4}} \quad \text{for } \nu = 0{\cdot}3. \tag{88}$$

6·3. *Beam of finite depth*

We have up to now considered the problem of a flange resting on a semi-infinite plate for the particular case $a = 0$, $A_b = \infty$. Before investigating the effects of different values of a and A_b, we shall first develop the analysis for a beam of finite depth. From physical considerations it is apparent that a beam of very large depth will be equivalent to a semi-infinite plate; what we have to determine is whether our simple analysis is sufficiently accurate for the depths of beam encountered in practice.

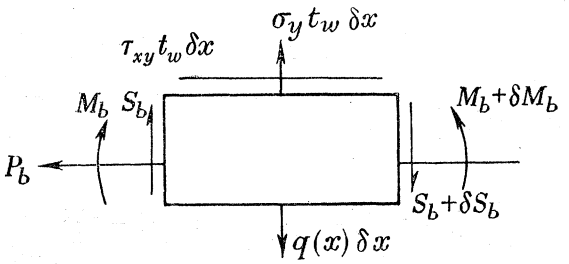

FIGURE 25. Equilibrium of an element of flange.

The beam is shown in figure 1, and from the equilibrium of an element of flange (figure 25) we have

$$\left.\begin{aligned} t_w\tau_{xy} &= A_b E\left\{\frac{\partial^2 u}{\partial x^2} - a\frac{\partial^3 v}{\partial x^3}\right\}, \\ t_w\sigma_y - q(x) &= -E(I_b + a^2A_b)\frac{\partial^4 v}{\partial x^4} + EaA_b\frac{\partial^3 u}{\partial x^3}. \end{aligned}\right\} \tag{89}$$

This time we apply the stress function

$$\phi = (C\cosh\alpha y + Dy\sinh\alpha y)\cos\alpha x \tag{90}$$

to the plate and obtain

$$\left.\begin{aligned}\sigma_x &= \{(C\alpha^2+2D\alpha)\cosh\alpha y + D\alpha^2 y\sinh\alpha y\}\cos\alpha x,\\ \sigma_y &= -(C\cosh\alpha y + Dy\sinh\alpha y)\,\alpha^2\cos\alpha x,\\ \tau_{xy} &= \{(C\alpha+D)\sinh\alpha y + D\alpha y\cosh\alpha y\}\,\alpha\sin\alpha x,\end{aligned}\right\} \tag{91}$$

and

$$\left.\begin{aligned}Eu &= \{\{C\alpha(1+\nu)+2D\}\cosh\alpha y + D\alpha(1+\nu)\,y\sinh\alpha y\}\sin\alpha x,\\ Ev &= -\{\{C\alpha(1+\nu)-D(1-\nu)\}\sinh\alpha y + D(1+\nu)\,\alpha y\cosh\alpha y\}\cos\alpha x,\end{aligned}\right\} \tag{92}$$

with rigid-body conditions $u = v = \mathrm{d}v/\mathrm{d}x = 0$ at the origin.

At $y = h$,

$$\left.\begin{aligned}Eu &= \{\{C\alpha(1+\nu)+2D\}\cosh\alpha h + D(1+\nu)\,\alpha h\sinh\alpha h\}\sin\alpha x,\\ Ev &= -\{\{C\alpha(1+\nu)-D(1-\nu)\}\sinh\alpha h + D(1+\nu)\,\alpha h\cosh\alpha h\}\cos\alpha x,\\ \sigma_y &= -\{C\cosh\alpha h + Dh\sinh\alpha h\}\,\alpha^2\cos\alpha x,\\ \tau_{xy} &= \{(C\alpha+D)\sinh\alpha h + D\alpha h\cosh\alpha h\}\,\alpha\sin\alpha x.\end{aligned}\right\} \tag{93}$$

Substituting (93) in (89) with $q(x) = \cos\alpha x$,

$$\left.\begin{aligned}C &= \frac{\begin{aligned}&[t_w(\sinh\alpha h+\alpha h\cosh\alpha h)+\alpha A_b(2\cosh\alpha h+\alpha h(1+\nu)\sinh\alpha h)\\ &\qquad -\alpha^2 A_b a\{(1+\nu)\,\alpha h\cosh\alpha h-(1-\nu)\sinh\alpha h\}]\end{aligned}}{\begin{aligned}&[-\alpha^3 t_w^2 h-\alpha^2 t_w^2\sinh\alpha h\cosh\alpha h-2A_b t_w\alpha^3\cosh^2\alpha h\\ &\quad +2A_b a t_w\alpha^4\{(1+\nu)\,\alpha h-(1-\nu)\sinh\alpha h\cosh\alpha h\}-2(I_b+a^2A_b)\,t_w\alpha^5\sinh^2\alpha h\\ &\quad +A_b I_b\alpha^6\{(1+\nu)^2\alpha h-(1+\nu)\,(3-\nu)\sinh\alpha h\cosh\alpha h\}]\end{aligned}},\\ D &= \frac{-\alpha t_w\sinh\alpha h-\alpha^2 A_b(1+\nu)\cosh\alpha h+\alpha^3 a A_b(1+\nu)\sinh\alpha h}{\text{same denominator}},\end{aligned}\right\} \tag{94}$$

whence

$$\sigma_y = \frac{-\alpha^2 t_w\sinh\alpha h\cosh\alpha h-\alpha^3 h t_w-2A_b\alpha^3\cosh^2\alpha h-A_b a\alpha^4\{(1-\nu)\sinh\alpha h\cosh\alpha h-(1+\nu)\,\alpha h\}}{\text{denominator of (94)}}, \tag{95}$$

which reduces to the same form as in equation (73) for large h.

Simplifying the expression by putting $a = 0$, $A_b = \infty$, we find on applying Fourier's integral theorem for a unit point load,

$$\sigma_y = \int_0^\infty \frac{1}{\pi t_w}\frac{\cos\alpha x\,\mathrm{d}\alpha}{1+\left\{\dfrac{(1+\nu)\,(3-\nu)}{2}\tanh\alpha h-\dfrac{(1+\nu)^2}{2}\dfrac{\alpha h}{\cosh^2\alpha h}\right\}\dfrac{\alpha^3 I_b}{t_w}} \tag{96}$$

(compare equation (75)).

The value of σ_y at $x = 0$ is plotted as a function of h in figure 26, where it will be seen that in the practical range there is little change from the value for the semi-infinite plate.

On integrating equation (96) twice we obtain the bending moment in the flange as

$$M_b - M_{b_0} = \int_0^\infty \frac{1}{\pi t_w\alpha^2}\frac{(1-\cos\alpha x)\,\mathrm{d}\alpha}{1+\left\{\dfrac{(1+\nu)\,(3-\nu)}{2}\tanh\alpha h-\dfrac{(1+\nu)^2}{2}\dfrac{\alpha h}{\cosh^2\alpha h}\right\}\dfrac{\alpha^3 I_b}{t_w}}-\frac{x}{2}, \tag{97}$$

whence, by a process similar to that used previously,

$$M_{b_0} = \int_0^\infty \frac{1}{\pi t_w} \frac{\left\{\frac{(1+\nu)(3-\nu)}{2}\tanh\alpha h - \frac{(1+\nu)^2}{2}\frac{\alpha h}{\cosh^2\alpha h}\right\}\frac{\alpha I_b}{t_w}}{1+\left\{\frac{(1+\nu)(3-\nu)}{2}\tanh\alpha h - \frac{(1+\nu)^2}{2}\frac{\alpha h}{\cosh^2\alpha h}\right\}\frac{\alpha^3 I_b}{t_w}} \mathrm{d}\alpha. \tag{98}$$

M_{b_0} is plotted as a function of h in figure 27. As with σ_y the values approximate closely to those for the semi-infinite plate, within the practical range. Accordingly we shall now return to the simpler analysis and assume that $h = \infty$ is sufficiently true for our purposes.

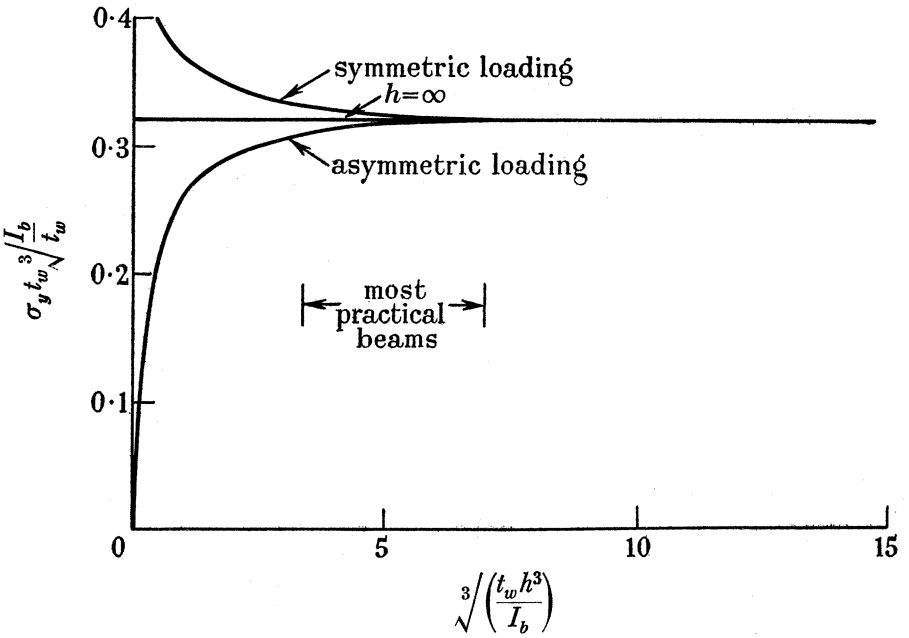

FIGURE 26. σ_y at $x = 0$ as a function of h.

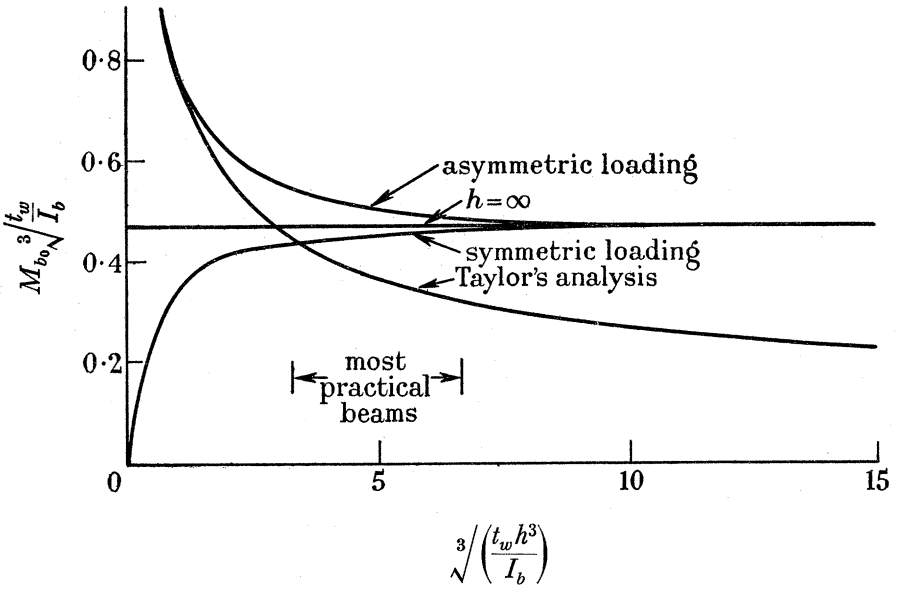

FIGURE 27. M_{b_0} as a function of h.

6·4. *Effects of various parameters*

From equations (73), the bending moment in the flange at the loading section,

$$M_{b_0} = -\int_0^\infty \frac{1}{\pi} \frac{2\alpha I_b + \alpha^2(1+\nu)(3-\nu)\frac{A_b I_b}{t_w}}{t_w + 2\alpha A_b + 2(1-\nu)\alpha^2 a A_b + 2\alpha^3(I_b + a^2 A_b) + \alpha^4(1+\nu)(3-\nu)\frac{A_b I_b}{t_w}} \mathrm{d}\alpha. \quad (99)$$

Two special cases can readily be evaluated. First, when $A_b/t_w^2 = 0$ or when $I_b/t_w^4 = \infty$, $A_b/t_w^2 \neq \infty$,

$$M_{b_0} = -\int_0^\infty \frac{1}{\pi} \frac{2\alpha I_b}{t_w + 2\alpha^3 I_b} \mathrm{d}\alpha$$

$$= -\frac{2}{3\sqrt{3}} \sqrt[3]{2}\, t_w \sqrt[3]{\frac{I_b}{t_w}}$$

$$= -0{\cdot}484 t_w \sqrt[3]{\frac{I_b}{t_w}}.* \quad (100)$$

Secondly, when $A_b/t_w^2 = \infty$, $a/t_w = 0$, $\nu = 0{\cdot}3$,

$$M_{b_0} = -0{\cdot}464 t_w \sqrt[3]{\frac{I_b}{t_w}} \quad (101)$$

from equation (86).

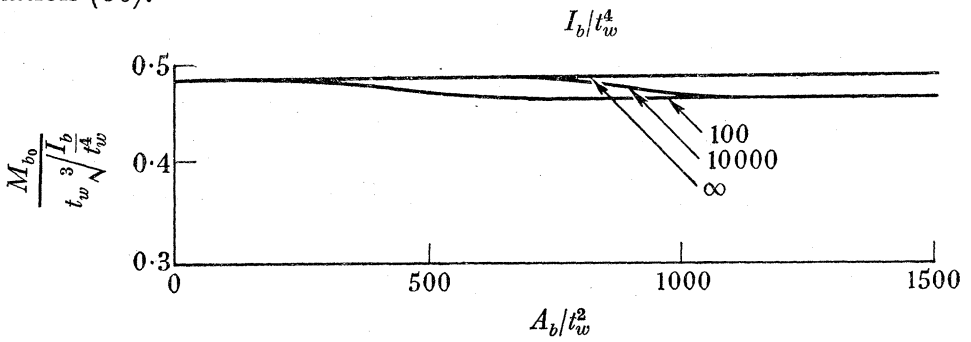

FIGURE 28. M_{b_0} for $a/t_w = 0$.

General curves of M_{b_0} for $a/t_w = 0$ and 10 are plotted in figures 28 and 29. It will be seen that for small values of a/t, $\frac{M_{b_0}}{t_w}\sqrt[3]{\frac{t_w^4}{I_b}}$ is practically independent of A_b/t_w^2 and I_b/t_w^4, as would be expected from the near correspondence of equations (100) and (101). For higher values of a/t_w, this is no longer true in general. For practical beams, however, large a/t_w are produced by small values of t_w, which in turn means that I_b/t_w^4 is large and the value of $\frac{M_{b_0}}{t_w}\sqrt[3]{\frac{t_w^4}{I_b}}$ approximates to the $I_b/t_w^4 = \infty$ solution, i.e. that given by equation (100).

We thus see that the bending moment in the flange at the loading section may be represented with reasonable accuracy by equation (100). This equation does in fact set an upper limit which will never quite be achieved in practice. Most practical beams fall about 10 % short of it. For example, the undercarriage girder discussed in part I gives $\frac{M_{b_0}}{t_w}\sqrt[3]{\frac{t_w^4}{I_b}} = 0{\cdot}422$. The results for the three mild steel experimental beams of part III are summarized in table 1.

* This equation also holds for the case of a flange resting on a smooth plate and has been deduced in the solution of this problem by Biot (1937).

TABLE 1

beam no.	a/t_w	A_b/t_w^2	I_b/t_w^4	$\frac{M_{b_0}}{t_w}\sqrt[3]{\frac{t_w^4}{I_b}}$
1	30	2700	810000	0·434
2	10	300	10000	0·422
3	3·3	33·3	123·5	0·424

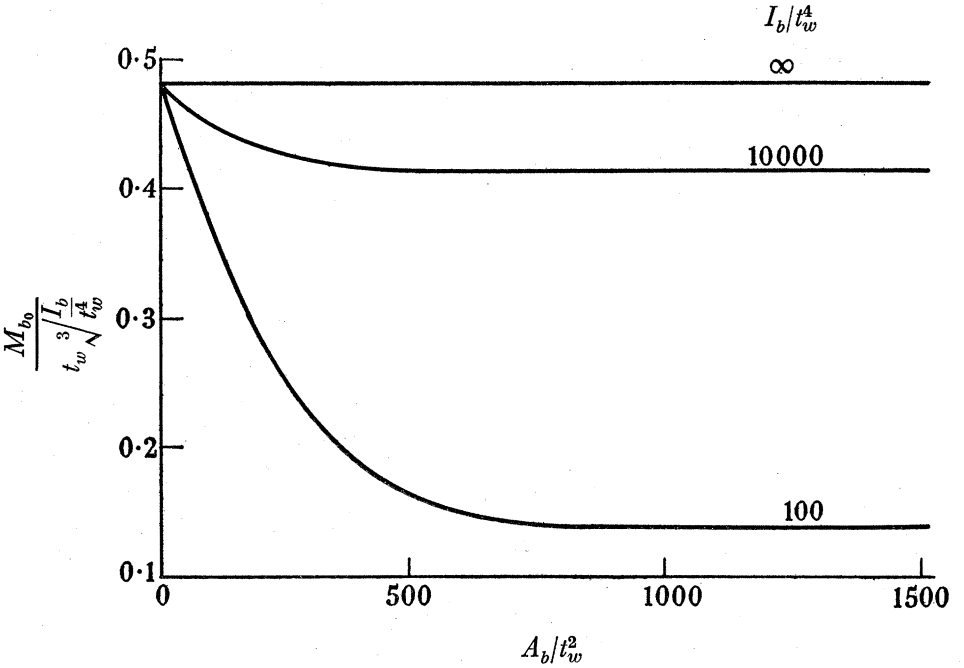

FIGURE 29. M_{b_0} for $a/t_w = 10$.

The end-load in the flange at the loading section may be obtained by the integration of equation (73) as

$$\frac{P_{b_0}t_w^2}{A_b} = \int_0^\infty \frac{t_w^2}{\pi} \frac{(1-\nu)+2\alpha a}{t_w+2\alpha A_b+2(1+\nu)\,\alpha^2 a A_b+2\alpha^3(I_b+a^2A_b)+\alpha^4(1+\nu)\,(3-\nu)\,\frac{A_bI_b}{t_w}}\,\mathrm{d}\alpha. \quad (102)$$

When $$\frac{A_b}{t_w^2}=\infty, \quad P_{b_0}\frac{t_w^2}{A_b}=0;$$

when $$\frac{A_b}{t_w^2}=0,$$

$$\frac{P_{b_0}t_w^2}{A_b} = \int_0^\infty \frac{(1-\nu)}{\pi}\frac{\mathrm{d}\alpha\, t_w}{1+\frac{2I_b}{t_w^4}\alpha^3t_w^3} + \frac{a}{t_w}\int_0^\infty \frac{2\alpha t_w}{\pi}\frac{\mathrm{d}\alpha\, t_w}{1+\frac{2I_b}{t_w^4}\alpha^3t_w^3}, \quad (103)$$

whence $$\frac{P_{b_0}t_w^2}{A_b}\sqrt[3]{\frac{I_b}{t_w^4}} = 0{\cdot}213+0{\cdot}484\,\frac{a}{t_w}\sqrt[3]{\frac{t_w^4}{I_b}}. \quad (104)$$

General curves of $\frac{P_{b_0}t_w^2}{A_b}\sqrt[3]{\frac{I_b}{t_w^4}}$ as a function of A_b/t_w^2 and I_b/t_w^4 are given in figures 30 and 31 for $a/t_w = 0$ and 10. It is not possible to develop a simple general formula for the determination of P_{b_0}, and if this function is required with any accuracy for values not covered by figures 30 and 31, it is best to calculate it directly from equation (102).

The outer fibre stress at the loading section may be written as

$$(\sigma_x)_H t_w^2 = \frac{b}{t_w}\left(\frac{t_w^4}{I_b}\right)^{\frac{1}{3}}\left[\frac{M_{b_0}}{t_w}\sqrt[3]{\frac{t_w^4}{I_b}}\right]+\left(\frac{t_w^4}{I_b}\right)^{\frac{1}{3}}\left[\frac{P_{b_0}t_w^2}{A_b}\sqrt[3]{\frac{I_b}{t_w^4}}\right], \tag{105}$$

where the terms in square brackets are the functions we have obtained previously.

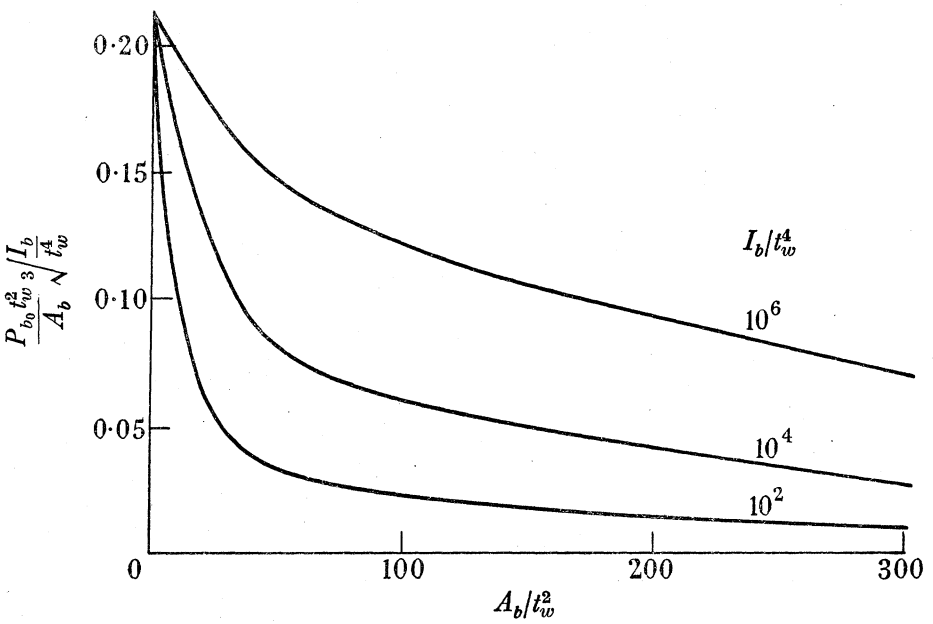

FIGURE 30. P_{b_0} for $a/t_w = 0$.

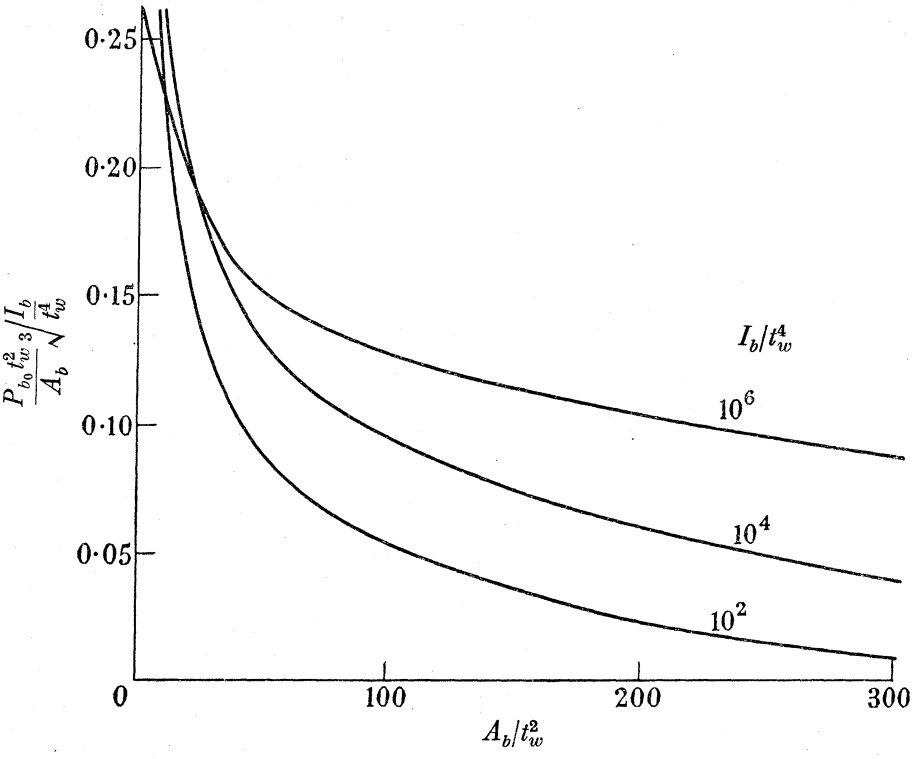

FIGURE 31. P_{b_0} for $a/t_w = 10$.

$\frac{M_{b_0}}{t_w}\sqrt[3]{\frac{t_w^4}{I_b}}$ is of the order of 80 to 90 % $\times$ 0·484. We have no general expression for $\frac{P_{b_0}t_w^2}{A_b}\sqrt[3]{\frac{I_b}{t_w^4}}$, but it is found that for practical beams with conventional rectangular or T-shaped flanges that the contribution of the end-load to the outer-fibre stress is 10 to 20 % of that of the bending moment and of the same sign. As a result, the sum of the two terms in equation (105) is found to approximate closely to $0{\cdot}484\frac{b}{t_w}\left(\frac{t_w^4}{I_b}\right)^{\frac{1}{3}}$. This correspondence is shown for the experimental beams of table 1 in table 2.

TABLE 2

beam no.	$\frac{a}{t_w}$	$\frac{b}{t_w}$	$\frac{A_b}{t_w^2}$	$\frac{I_b}{t_w^4}$	$\frac{M_{b_0}}{t_w}\sqrt[3]{\frac{t_w^4}{I_b}}$	$\frac{P_{b_0}t_w^2}{A_b}\sqrt[3]{\frac{I_b}{t_w^4}}$	$\frac{M_{b_0}bt_w^2}{I_b}$	$\frac{P_{b_0}t_w^2}{A_b}$	$(\sigma_x)_H\,t_w^2$	$0{\cdot}484\frac{b}{t_w}\left(\frac{t_w^4}{I_b}\right)^{\frac{1}{3}}$
1	30	30	2700	810000	0·434	0·0195	0·00150	0·00021	0·00171	0·00168
2	10	10	300	10000	0·422	0·0391	0·0090	0·0018	0·0108	0·0105
3	3·3̇	3·3̇	33·3̇	123·5	0·424	0·0622	0·057	0·012	0·069	0·065

We thus see that for most practical beams we may express the outer-fibre stress at the loading section due to two symmetric loads W applied to the flanges as

$$(\sigma_x)_H = 0{\cdot}484\frac{W}{t_w^2}\frac{b}{t_w}\left(\frac{t_w^4}{I_b}\right)^{\frac{1}{3}}. \tag{106}$$

For beams of very unusual section it may be advisable to consult figures 28 to 31 or to calculate from equations (99) and (102).

7. Equal and similar loads on the flanges

In § 6 we saw that the outer-fibre stress produced by the application of two equal and opposite loads to the flanges was substantially the same as that produced by the application of a single load to a flange resting on a semi-infinite plate. We now proceed to determine whether a similar correspondence is obtained when the loads are in the same direction.

The beam is again as shown in figure 1 and from the equilibrium of an element (figure 25) we obtain the same equations (89). This time, however, we apply the stress function

$$\phi = (C\sinh\alpha y + Dy\cosh\alpha y)\cos\alpha x \tag{107}$$

to the plate. The subsequent analysis is similar to that of § 6, and for $a = 0$, $A_b = \infty$ and a point load we get

$$\sigma_y = \int_0^\infty \frac{1}{\pi t_w}\frac{\cos\alpha x\,\mathrm{d}\alpha}{1+\left\{\frac{(1+\nu)(3-\nu)}{2}\coth\alpha h + \frac{(1+\nu)^2}{2}\frac{\alpha h}{\sinh^2\alpha h}\right\}\frac{\alpha^3 I_b}{t_w}}. \tag{108}$$

The value of σ_y at $x = 0$ is plotted as a function of h in figure 26, and once again there is little change from the $h = \infty$ values in the practical range.

The bending moment in the flange at the origin is given by

$$M_{b_0} = \int_0^\infty \frac{1}{\pi t_w}\frac{\left\{\frac{(1+\nu)(3-\nu)}{2}\coth\alpha h + \frac{(1+\nu)^2}{2}\frac{\alpha h}{\sinh^2\alpha h}\right\}\frac{\alpha I_b}{t_w}}{1+\left\{\frac{(1+\nu)(3-\nu)}{2}\coth\alpha h + \frac{(1+\nu)^2}{2}\frac{\alpha h}{\sinh^2\alpha h}\right\}\frac{\alpha^3 I_b}{t_w}}\mathrm{d}\alpha, \tag{109}$$

and this is plotted as a function of h in figure 27. As with σ_y the values are close to those for the semi-infinite plate.

We thus see that both for symmetric and asymmetric loading the theory for the flange resting on a semi-infinite plate may be applied with sufficient accuracy to the beam of finite depth, and since any type of flange loading can be obtained by suitable combination of these two solutions, we can write quite generally, for the outer fibre stress in the loaded flange at the loading section due to a load W applied to one flange of a beam,

$$(\sigma_x)_H = (\sigma_x)_{H\,\text{eng.}} + 0{\cdot}484\,\frac{W}{t_w^2}\,\frac{b}{t_w}\left(\frac{t_w^4}{I_b}\right)^{\frac{3}{8}}. \tag{110}$$

8. Full analysis applied to a numerical example

It will be remembered that in deriving the fact that beam depth, h, has little effect on outer-fibre stress, we made use of the simplifying assumption $a = 0$, $A_b = \infty$. It is proposed now to investigate an example in which a and A_b have finite values, to check that the semi-infinite plate solution is still a good approximation to that for the practical beam. The analysis is developed quite generally, but numerical application is limited to the under-carriage girder of figure 2.

For the symmetric loading case,

$$\tau_{xy} = \frac{1}{\pi}\int_0^\infty \frac{2\alpha^2 aA_b\sinh^2\alpha h - \alpha^2 hA_b(1+\nu) + (1-\nu)\,\alpha A_b\sinh\alpha h\cosh\alpha h}{\begin{aligned}&[-t_w^2\alpha h - t_w^2\sinh\alpha h\cosh\alpha h - 2A_b t_w\alpha\cosh^2\alpha h\\ &+t_w aA_b\alpha^2\{2(1+\nu)\,\alpha h - 2(1-\nu)\sinh\alpha h\cosh\alpha h\} - 2\{I_b + a^2A_b\}t_w\alpha^3\sinh^2\alpha h,\\ &+A_b I_b\alpha^4\{(1+\nu)^2\alpha h - (1+\nu)\,(3-\nu)\sinh\alpha h\cosh\alpha h\}]\end{aligned}}\sin\alpha x\,\mathrm{d}\alpha, \tag{111}$$

and on integrating

$$P_{b_0} = \frac{t_w}{\pi}\int_0^\infty \frac{2\alpha aA_b\sinh^2\alpha h - \alpha hA_b(1+\nu) + (1-\nu)\,A_b\sinh\alpha h\cosh\alpha h}{\text{denominator of (111)}}\mathrm{d}\alpha. \tag{112}$$

Further,

$$\sigma_y = -\frac{1}{\pi}\int_0^\infty \frac{\begin{aligned}&[t_w\alpha h + t_w\sinh\alpha h\cosh\alpha h + 2A_b\alpha\cosh^2\alpha h\\ &+aA_b\{-(1+\nu)\,\alpha^3 h + (1-\nu)\,\alpha^2\sinh\alpha h\cosh\alpha h\}]\end{aligned}}{\text{denominator of (111)}}\cos\alpha x\,\mathrm{d}\alpha \tag{113}$$

and

$$M_{b_0} = P_{b_0}a + \frac{1}{\pi}\int_0^\infty \frac{\begin{aligned}&[A_b at_w\{-(1+\nu)\,\alpha h + (1-\nu)\sinh\alpha h\cosh\alpha h\} + 2\{I_b + a^2A_b\}t_w\alpha\sinh^2\alpha h\\ &+A_b I_b\alpha^2\{-(1+\nu)^2\alpha h + (1+\nu)\,(3-\nu)\sinh\alpha h\cosh\alpha h\}]\end{aligned}}{\text{denominator of (111)}}\mathrm{d}\alpha. \tag{114}$$

For the asymmetric loading case

$$\tau_{xy} = \frac{1}{\pi}\int_0^\infty \frac{2\alpha^2 aA_b\cosh^2\alpha h + \alpha^2 h(1+\nu)\,A_b + (1-\nu)\,\alpha A_b\sinh\alpha h\cosh\alpha h}{\begin{aligned}&[t_w^2\alpha h - t_w^2\sinh\alpha h\cosh\alpha h - 2A_b t_w\sinh^2\alpha h\\ &-t_w aA_b\alpha^2\{2(1+\nu)\,\alpha h + 2(1-\nu)\sinh\alpha h\cosh\alpha h\} - 2\{I_b + a^2A_b\}t_w\alpha^3\cosh^2\alpha h\\ &-A_b I_b\alpha^4\{(1+\nu)^2\alpha h + (1+\nu)\,(3-\nu)\sinh\alpha h\cosh\alpha h\}]\end{aligned}}\sin\alpha x\,\mathrm{d}\alpha. \tag{115}$$

Now when x is large, we are interested in small α only, so

$$\begin{aligned}\tau_{xy} &= -\frac{2}{\pi t_w}\int_0^\infty \frac{A_b(a+h)}{2I_b + 2A_b(a+h)^2 + \frac{2}{3}t_w h^3}\,\frac{\sin\alpha x}{\alpha}\,\mathrm{d}\alpha\\ &= -\frac{1}{t_w}\,\frac{A_b(a+h)}{2I_b + 2A_b(a+h)^2 + \frac{2}{3}t_w h^3},\end{aligned} \tag{116}$$

the engineers' theory value.

The end-load due to stress concentration,

$$P_{b_0} = \frac{t_w}{\pi}\int_0^\infty \left\{ \frac{2\alpha a A_b \cosh^2 \alpha h + \alpha h A_b(1+\nu) + (1-\nu) A_b \sinh \alpha h \cosh \alpha h}{\text{denominator of (115)}} + \frac{2A_b(a+h)}{\alpha^2 t_w \{2I_b + 2A_b(a+h)^2 + \frac{2}{3}t_w h^3\}} \right\} \mathrm{d}\alpha. \tag{117}$$

The transverse stress

$$\sigma_y = -\frac{1}{\pi}\int_0^\infty \frac{[-t_w \alpha h + t_w \sinh \alpha h \cosh \alpha h + 2A_b \alpha \sinh^2 \alpha h + aA_b\{(1+\nu)\alpha^3 h + (1-\nu)\alpha^2 \sinh \alpha h \cosh \alpha h\}]}{\text{denominator of (115)}} \cos \alpha x \, \mathrm{d}\alpha, \tag{118}$$

and the shear in the boom due to stress concentration

$$S_b = -\frac{t_w}{\pi}\int_0^\infty \frac{[-t_w \alpha h + t_w \sinh \alpha h \cosh \alpha h + 2A_b \alpha \sinh^2 \alpha h + aA_b\{(1+\nu)\alpha^3 h + (1-\nu)\alpha^2 \sinh \alpha h \cosh \alpha h\}]}{\text{denominator of (115)}} \frac{\sin \alpha x \, \mathrm{d}\alpha}{\alpha} - \frac{h\{A_b(a+h) + \frac{1}{3}h^2 t\}}{2I_b + 2A_b(a+h)^2 + \frac{2}{3}t_w h^3}, \tag{119}$$

where the last term represents the shear at $x = 0$. It should be noted that it is not $-\frac{1}{2}$, since engineers' theory accounts for

$$\frac{I_b + A_b a(a+h)}{2I_b + 2A_b(a+h)^2 + \frac{2}{3}t_w h^3}.$$

This difference ensures that S_b tends to zero for large x.

The bending moment in the flange at the loading section can be obtained in the usual way as

$$M_{b_0} = P_{b_0} a + \frac{1}{\pi}\int_0^\infty \left\{ \frac{[A_b a t_w\{(1+\nu)\alpha h + (1-\nu)\sinh \alpha h \cosh \alpha h\} + 2\{I_b + a^2 A_b\} t_w \alpha \cosh^2 \alpha h + A_b I_b \alpha^2\{(1+\nu)^2 \alpha h + (1+\nu)(3-\nu)\sinh \alpha h \cosh \alpha h\}]}{\text{denominator of (115)}} - \frac{2A_b a(a+h) + 2I_b}{\alpha^2\{2I_b + 2A_b(a+h)^2 + \frac{2}{3}t_w h^3\}} \right\} \mathrm{d}\alpha. \tag{120}$$

On substituting the numerical values appropriate to the undercarriage girder in equations (99), (102), (110), (112), (114), (117) and (120) we get the comparisons of table 3.

TABLE 3

loading condition and type of analysis	M_{b_0} Lb.in./Lb.	P_{b_0} Lb./Lb.	$(\sigma_x)_H$ Lb./in.^{2}/Lb.
semi-infinite plate exact analysis	0·907	−0·546	0·817
symmetric loading exact analysis	0·731	−0·131	0·556
asymmetric loading exact analysis	0·946	−0·004	0·663
simple formula	1·042	0	0·729

It will be noted that the bending moment for symmetric loading of a beam of finite depth is less than that for the semi-infinite plate, and that for asymmetric loading it is greater, as

predicted by figure 27. The decreases in P_{b_0} for the beam of finite depth can be predicted by considering end-load equilibrium for the symmetric loading case, and moment equilibrium for the asymmetric case. The simple formula gives an estimate of the outer-fibre stress somewhat in excess of the true values.

By adding together the symmetric and asymmetric loadings in equal proportions we obtain the case of load applied to one flange only. The total stresses in the flanges of the undercarriage girder for this type of loading and $L/h = 5$ are shown in figure 10. They are compared with those due to engineers' theory and the analysis of part I. It will be seen that the stresses in the unloaded flange are similar to those obtained when the load is applied through the web; this is to be expected since the only local perturbations (those due to making $S_b = \tau_{xy} = 0$) are the same in both cases.

PART III. EXPERIMENTAL EVIDENCE

9. Experimental results

As a means of providing some practical check on the preceding analyses, three mild steel beam specimens were obtained; their cross-sections are given in figure 32. Electrical resistance strain gauges were affixed to the inner and outer faces of the booms and these were calibrated *in situ* by applying four-point loading (pure bending) well away from the strain-gauged sections.

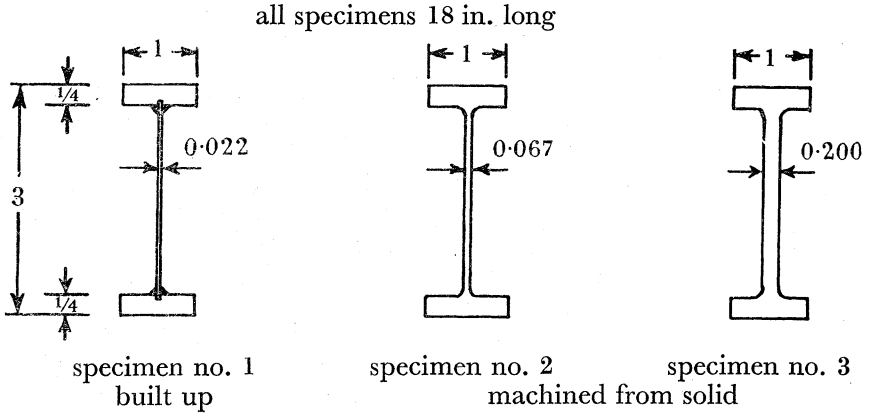

Figure 32. Experimental beams.

The method of determining the stress concentrations was as follows. Suppose that under pure bending a gauge reading (percentage change of resistance) per unit bending moment is R_1 and that under any other form of loading it is R_2. Then the stress concentration, which we will denote by $(\sigma_x)_s$ is given by

$$(\sigma_x)_s = \left(\frac{R_2}{R_1} - 1\right)(\sigma_x)_{\text{eng.}}. \tag{121}$$

It will be noted that this method of calculation depends only on the assumption that engineers' theory gives the stresses correctly when the beam is subjected to pure bending: it does not depend on any knowledge of the gauge calibration constant and errors due to

such causes as incomplete adhesion of the gauge and dead resistance in the bridge circuit are largely eliminated.

In the experiments to check the analysis of part I, the beams were loaded by means of friction clamps attached to the webs. These are shown, together with a general arrangement of the test rig in figure 33. Each specimen was tested for a short and a long span ($L/h = 3{\cdot}5$ and $6{\cdot}5$) and the values of $(\sigma_x)_s$ obtained are compared with the theoretical curves in figure 34. Figure 35 shows the experimental results for the thin web specimen under the short-span loading compared with the theoretical stresses according to engineers' theory and according to the analysis of part I. It will be seen that in this extreme case engineers' theory not only predicts the wrong magnitude for the stresses on the inner face of the boom, but is actually wrong in sign.

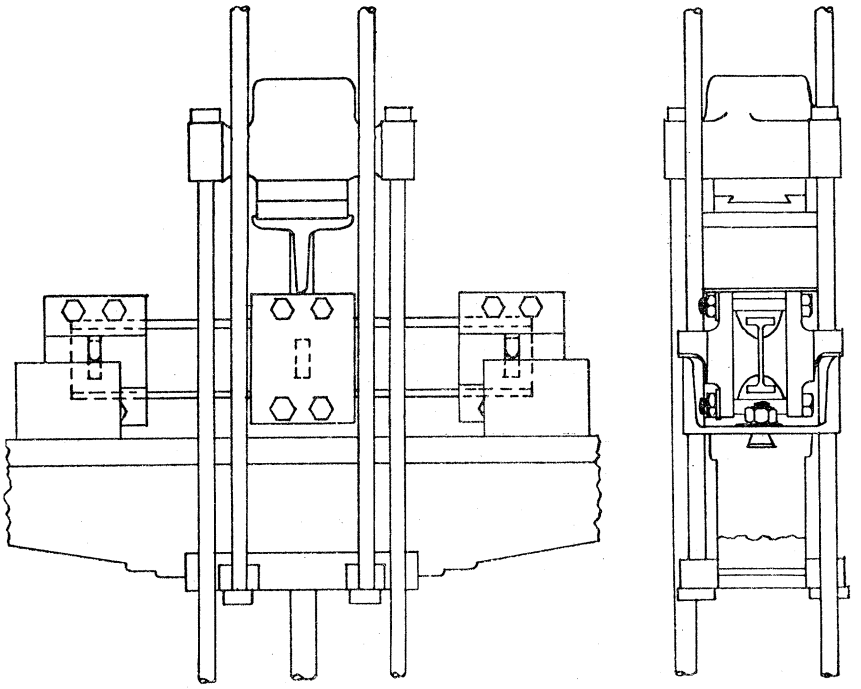

FIGURE 33. General arrangement of test rig, showing three-point loading applied to web.

A second set of experiments was carried out (for $L/h = 4{\cdot}25$ only) in which the beams were subjected to equal and similar flange loads by means of the rig shown in figure 36. (The rods are pre-compressed and then the incremental loads are applied equally to each flange because the cross-beams are very flexible vertically compared with the rods.) The results are compared with the theoretical curves due to the simplified analysis of part II in figure 37.

Finally, the medium web specimen only was tested for $L/h = 3{\cdot}5$ with the load applied to one flange only. The stresses obtained are compared with those from the full analysis of § 6·3 in figure 38.

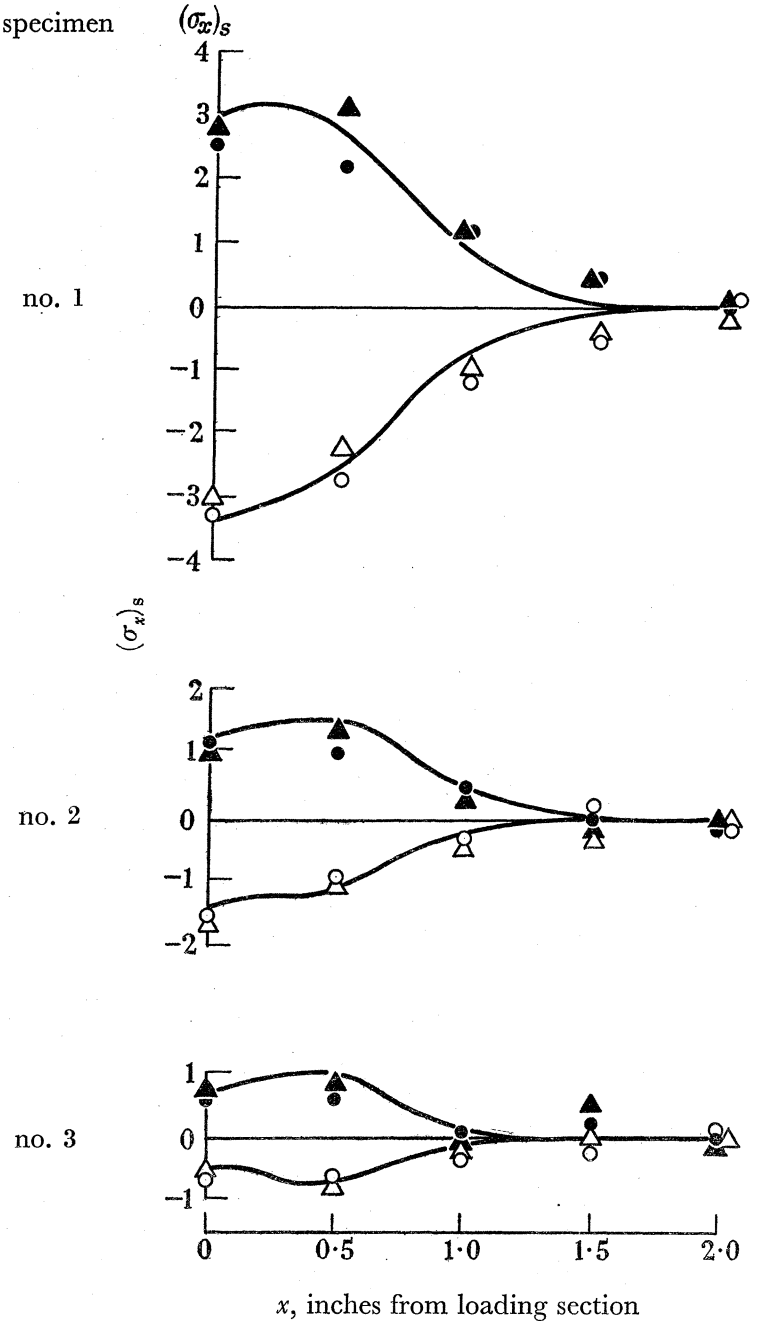

FIGURE 34. Theoretical and experimental values of $(\sigma_x)_s$ for mild steel beams loaded through the web. The stress concentrations are plotted to such a scale that the engineers' theory outer fibre stress is unity at the loading section for $L/h = 1$.

	theoretical	experimental $L/h = 3{\cdot}5$	experimental $L/h = 6{\cdot}5$
outer face of boom	upper line	●	▲
inner face of boom	lower line	○	△

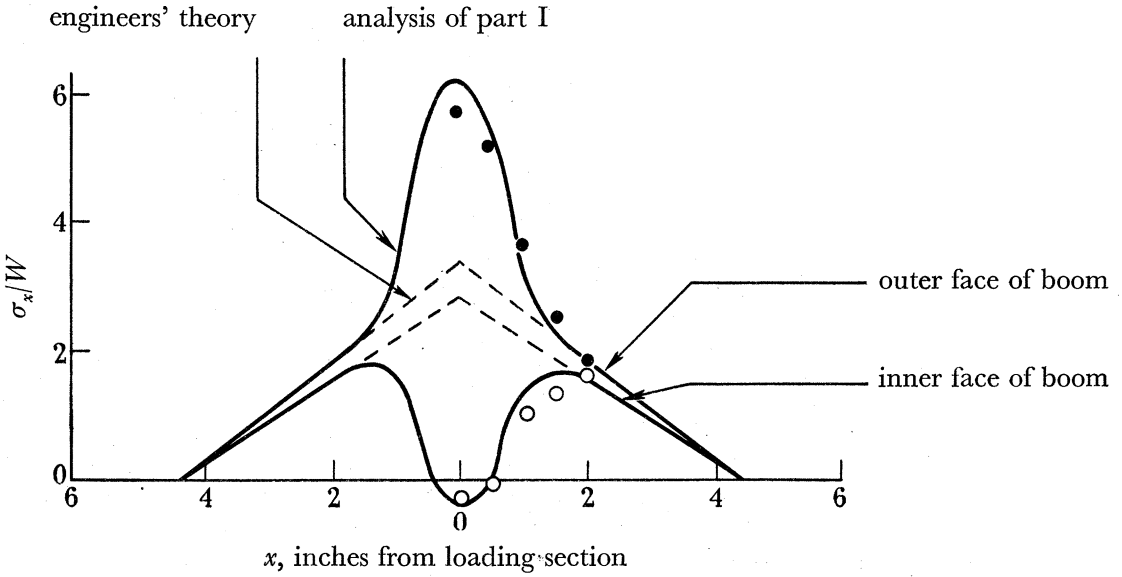

FIGURE 35. Stresses in specimen no. 1. $L/h = 3{\cdot}5$, web loading.

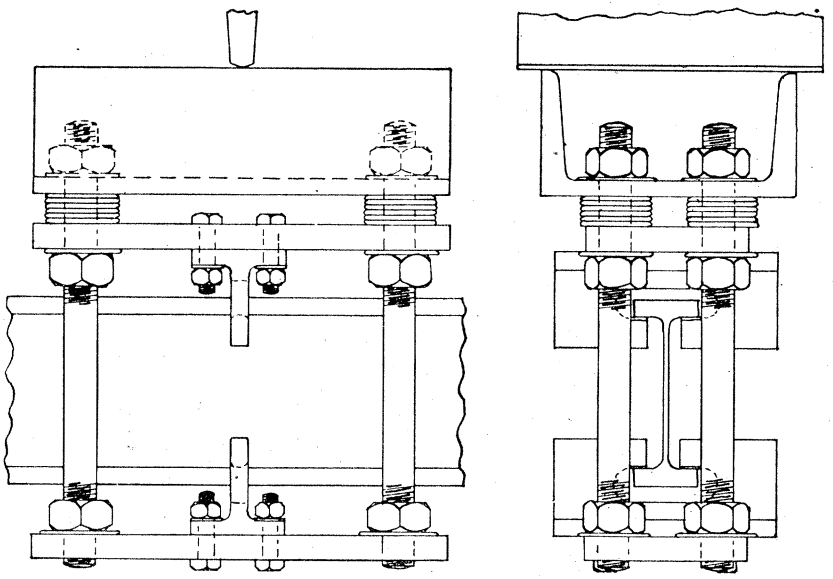

FIGURE 36. Rig for applying equal loads to flanges.

10. STATISTICAL ANALYSIS OF THE RESULTS

Strain-gauge readings as taken during a structural test are nearly always in the form of a table or graph of percentage change of resistance (measured on the bridge circuit) against applied load (measured on the testing machine). The load application is in general more accurate than the strain-gauge readings and so in the following analysis we shall assume that the applied load (W) is our independent variate and that all the error occurs in the percentage change of resistance (r).

Let us suppose that there are μ readings at equal intervals of load w, as shown in figure 39.

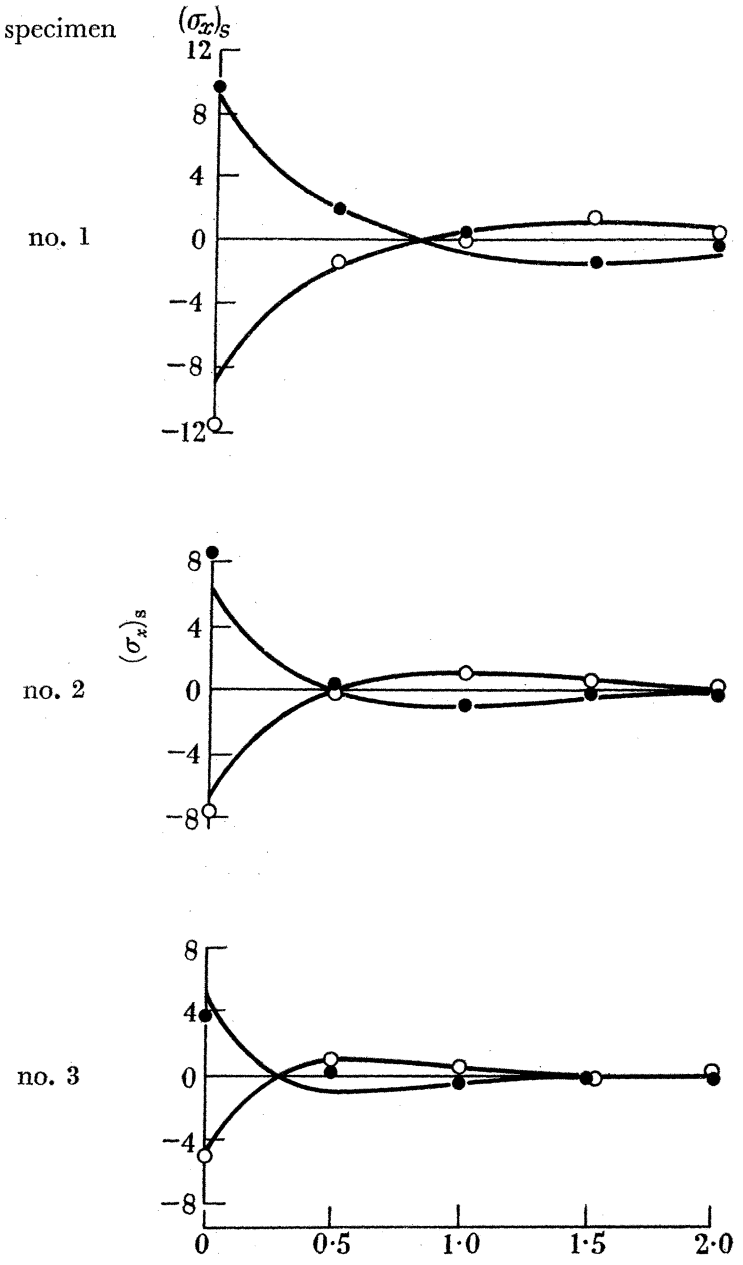

FIGURE 37. Theoretical and experimental values of $(\sigma_x)_s$ for mild steel beams with two equal loads applied to the flanges. The stress concentrations are plotted to such a scale that the engineers' theory outer fibre stress is unity at the loading section for $L/h=1$. The upper lines (at $x=0$) refer to the outer face of the boom and the lower to the inner. All tests carried out at $L/h=4{\cdot}25$. Experimental results: ●○. The theoretical curves are derived from the simplified analysis of part II, §6·2.

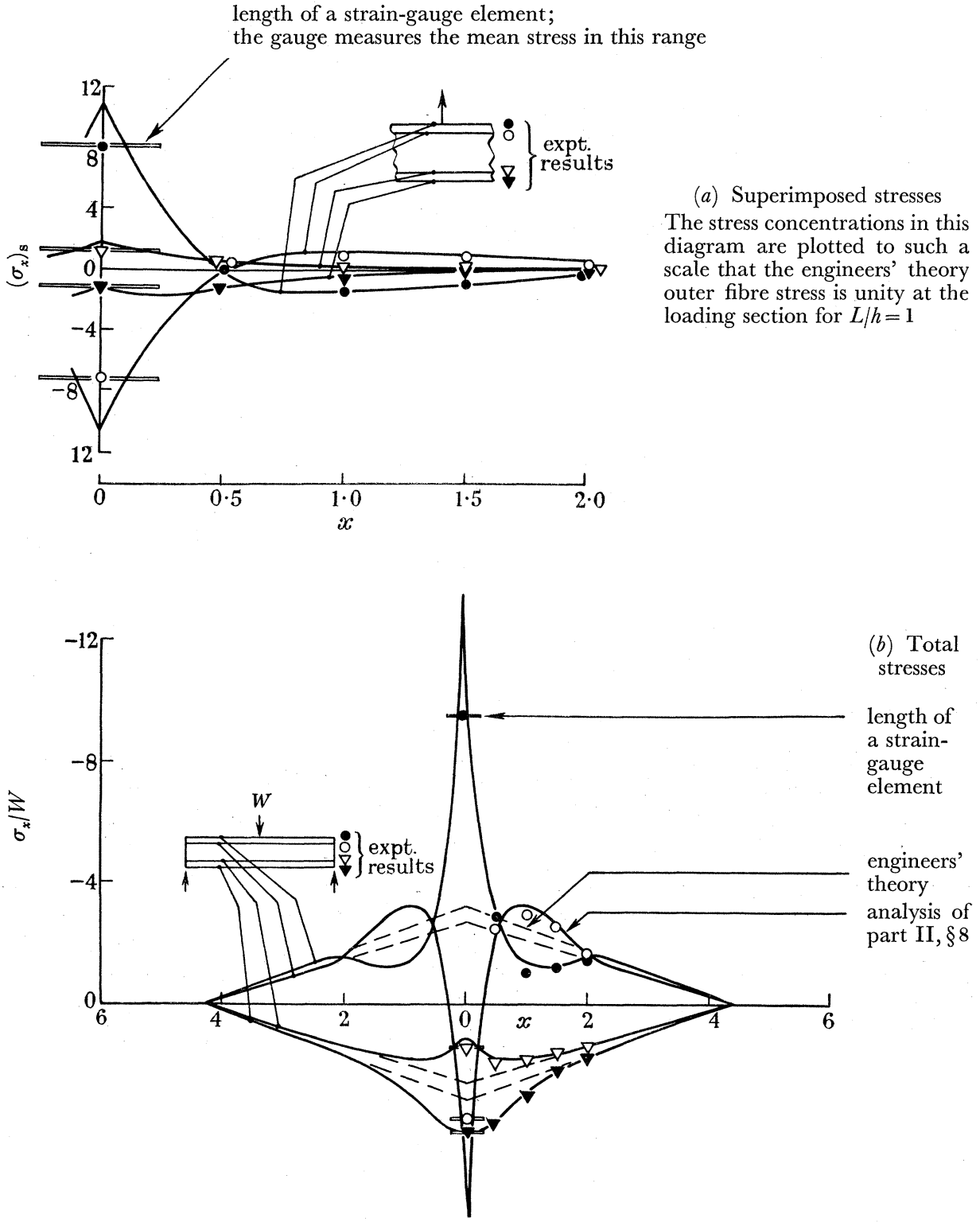

FIGURE 38. Stresses in specimen no. 2, $L/h = 3{\cdot}5$, with load applied to one flange. The theoretical curves are derived from the full analysis of § 8.

A regression line of slope θ can be fitted to these results by means of the method of least squares, i.e. the line is given by the equation

$$r = \xi + \theta W, \tag{122}$$

where

$$\left.\begin{aligned} \theta &= \frac{\Sigma(W-\overline{W})\,(r-\bar{r})}{\Sigma(W-\overline{W})^2}, \\ \xi &= \bar{r} - \theta\overline{W}, \end{aligned}\right\} \tag{123}$$

the bars referring to arithmetic means. This particular line has the property that the sum of the squares of the deviations of r from it is a minimum.

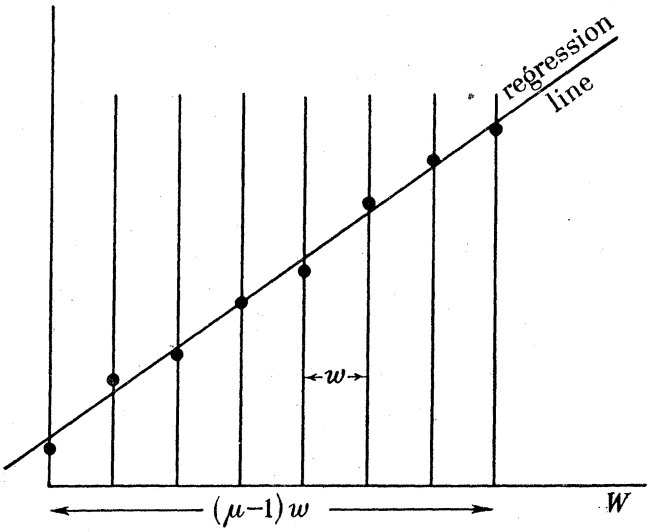

FIGURE 39. Strain-gauge readings.

Then the variance of r about the regression line is independent of W and equal to ψ_r^2, the universe variance for the particular type of strain gauge and circuit used. ψ_r^2 may be known from previous experience or an estimate of it may be made from

$$q_r^2 = \frac{\sum_1^{\mu}\{r-\xi-\theta W\}^2}{\mu-2}. \tag{124}$$

The factor $\mu-2$ is used to give an unbiased estimate, rather than μ, because two of the degrees of freedom of the system have already been used up in obtaining the regression line.

The standard deviation of θ is given by

$$\psi_\theta = \psi_r/\{\Sigma(W-\overline{W})^2\}^{\frac{1}{2}} \tag{125}$$

$$= \frac{\psi_r}{w}\left\{\frac{12}{\mu(\mu^2-1)}\right\}^{\frac{1}{2}}, \tag{126}$$

and thus the coefficient of variation

$$\frac{\psi_\theta}{\theta} = \frac{\psi_r}{r_{\text{tot.}}}\left\{\frac{12(\mu-1)}{\mu(\mu+1)}\right\}^{\frac{1}{2}}, \tag{127}$$

where $r_{\text{tot.}}$ is the total range of r.

Having a value for reading per unit load we shall next require to obtain a value for reading per unit bending moment at the section considered. Assuming as before that W is known accurately, the errors in the bending moment will depend on the errors in the geometry of the loading system (inaccuracies in the position of the clamps, the difficulty of defining exactly where the load acts on the bearing surface, etc.). If the standard deviation of any measurement of length is ψ_x, it may be shown that for pure bending

$$\frac{\psi_M}{M} = \sqrt{\frac{19}{2}}\frac{\psi_x}{L}, \tag{128}$$

where L is the distance between the loading points, and for the centrally loaded beam,

$$\frac{\psi_M}{M} = \sqrt{\frac{7}{2}}\frac{\psi_x}{L}, \tag{129}$$

where L is the semi-span.

The coefficient of variation for reading per unit bending moment can now be obtained as

$$\lambda_R = \left\{\left(\frac{\psi_\theta}{\theta}\right)^2 + \left(\frac{\psi_M}{M}\right)^2\right\}^{\frac{1}{2}}. \tag{130}$$

Having the coefficients of variation for R_1 and R_2, the readings per unit bending moment under pure bending and central loading respectively, we find from equation (121)

$$\lambda\{(\sigma_x)_s + (\sigma_x)_{\text{eng.}}\} = \{\lambda_{R_1}^2 + \lambda_{R_2}^2\}^{\frac{1}{2}}. \tag{131}$$

Now $(\sigma_x)_{\text{eng.}}$ depends on assumed geometric properties only and so introduces no further error, whence

$$\psi\{(\sigma_x)_s = \{\lambda_{R_1}^2 + \lambda_{R_2}^2\}^{\frac{1}{2}}\{(\sigma_x)_s + (\sigma_x)_{\text{eng.}}\}. \tag{132}$$

In the actual experimental work $(\sigma_x)_s$ was generally small compared with $(\sigma_x)_{\text{eng.}}$, so we may write

$$\psi(\sigma_x)_s = \{\lambda_{R_1}^2 + \lambda_{R_2}^2\}^{\frac{1}{2}}(\sigma_x)_{\text{eng.}}. \tag{133}$$

In plotting the results, the experimental values of $(\sigma_x)_s$ have been multiplied by L/h and we have made $(\sigma_x)_{\text{eng.}}$ approximately equal to unity, whence

$$\psi(\sigma_x)_s = \frac{L}{h}\{\lambda_{R_1}^2 + \lambda_{R_2}^2\}^{\frac{1}{2}}. \tag{134}$$

As an example we consider the following figures obtained for the same gauge of specimen no. 2 under (a) a test with pure bending and (b) a test with central loading:

	(a)	(b)
$r_{\text{tot.}}$	0·120	0·060
ψ_r	0·02	0·02
μ	16	12
ψ_θ/θ	0·0136	0·0307
ψ_x	0·02	0·02
L	4·375	4·375
ψ_M/M	0·0141	0·0086
λ_{R_1}	0·0196	0·0319

Combining these

$$\psi(\sigma_x)_s = 3{\cdot}5\{0{\cdot}0196^2 + 0{\cdot}0319^2\}^{\frac{1}{2}}$$
$$= 0{\cdot}131. \tag{135}$$

Now tests have generally been carried out to about the same total load (except for the pure bending calibration tests which were taken higher to ensure accuracy) and with the same load increments, so that the effect of increasing L/h is to decrease ψ_θ/θ and ψ_M/M and therefore λ_{R_2} proportionately. λ_{R_1}, the pure bending calibration value, remains unchanged, but since it is smaller than λ_{R_2} the net effect is still to decrease $\{\lambda_{R_1}^2 + \lambda_{R_2}^2\}^{\frac{1}{2}}$ roughly as h/L, and so we find that variations in L/h produce little change in $\psi(\sigma_x)_s$. Similarly, $\psi(\sigma_x)_s$ is about the same for all the specimens, since these were of the same depth, almost the same second moments of area, and were similarly strain gauged.

The results of a number of calculations of $\psi(\sigma_x)_s$ similar to the one set out above have shown that for all our experimental results we may with sufficient accuracy take

$$\psi(\sigma_x)_s = 0{\cdot}15. \tag{136}$$

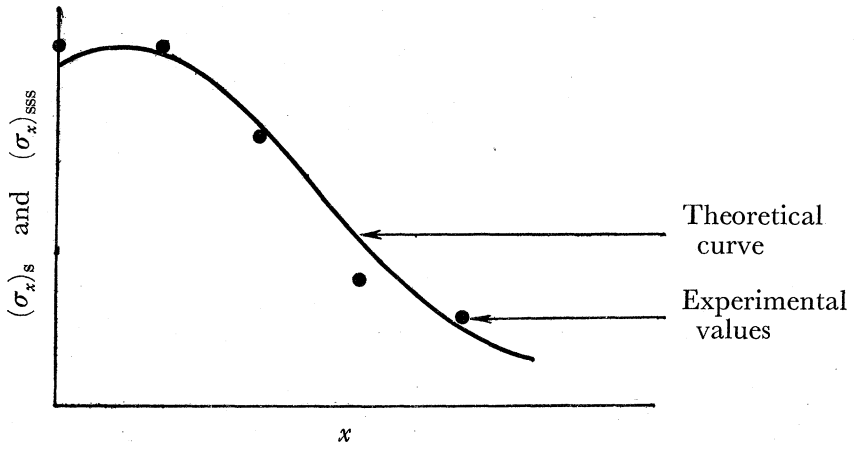

FIGURE 40. Stress concentrations, theoretical curve and experimental values.

Turning now to the comparison of the theoretical curves with the experimental values of $(\sigma_x)_s$, let there be p observations $(\sigma_x)_s$ and let the corresponding theoretical values for the same x be $(\sigma_x)_{sss}$ (figure 40). We assume x to be the independent variate and we set up the null hypothesis that $\{(\sigma_x)_s - (\sigma_x)_{sss}\}$ are a set of observations drawn from a universe of mean zero and standard deviation $\psi(\sigma_x)_s$. Then the experimental arithmetic mean is

$$\frac{\Sigma\{(\sigma_x)_s - (\sigma_x)_{sss}\}}{p} = \rho, \tag{137}$$

and the experimental standard deviation is

$$\left\{\frac{\Sigma\{(\sigma_x)_s - (\sigma_x)_{sss}\}^2}{p}\right\}^{\frac{1}{2}} = q. \tag{138}$$

It may be noted that the divisor in the second equation is p, not $p-1$, since we are using an arithmetic mean of zero, not ρ.

Now, using the 5 % significance limits as our criteria,

$$\left.\begin{aligned} &\rho \text{ should not exceed } t_s \psi(\sigma_x)_s, \\ &q \text{ should not exceed } \sqrt{(F_s)}\, \psi(\sigma_x)_s, \end{aligned}\right\} \tag{139}$$

where t_s is 'Student's' ratio depending on the number of degrees of freedom of $\psi(\sigma_x)_s$ (∞ in the present example) and F_s is a function depending on the number of degrees of freedom of q and $\psi(\sigma_x)_s$ (p and ∞ in the present example) (see Davies 1949).

Table 4 gives the values of ρ and q for the mild steel experimental beams.

TABLE 4

Tests with load applied to the web (figure 34)

		L/h	ρ	q
specimen no. 1:	outer fibre	3·5	−0·03	0·38
		6·5	0·23	0·34
	inner fibre	3·5	−0·18	0·32
		6·5	−0·05	0·30
specimen no. 2:	outer fibre	3·5	−0·14	0·22
		6·5	−0·11	0·12
	inner fibre	3·5	0·01	0·13
		6·5	−0·10	0·13
specimen no. 3:	outer fibre	3·5	−0·11	0·22
		6·5	−0·01	0·22
	inner fibre	3·5	−0·06	0·13
		6·5	0	0·04

Test of specimen no. 2 *with load applied to one flange* (figure 38)

		ρ	q
loaded flange:	outer fibre	0·11	0·21
	inner fibre	0·10	0·20
unloaded flange:	outer fibre	0·11	0·15
	inner fibre	0·12	0·20

No attempt has been made to analyze the results for the equal-flange loadings shown in figure 37, since the theoretical curves are those due to the simplified analysis. The full analysis has not been applied to all the cases of flange loading, owing to the very heavy arithmetic work involved.

For each of the values of ρ and q quoted above, p has a value of 5, so that we must use the values of t_s and F_s appropriate to (5) and (5,∞), i.e. 1·96 and 2·21. Accordingly the maximum permissible values to satisfy the 5 % significance limits are

$$\left.\begin{aligned} \rho &= 1{\cdot}96\psi(\sigma_x)_s = 0{\cdot}29, \\ q &= 1{\cdot}49\psi(\sigma_x)_s = 0{\cdot}22. \end{aligned}\right\} \tag{140}$$

It will be seen that all the results satisfy these values with exception of specimen no. 1 under web loading. Here the mean value is satisfactory, but there is an abnormal scatter. This may be attributed to the method of manufacture. Specimens nos. 2 and 3 were machined from solid black bar and were free from warping. Specimen no. 1 had too thin a web for this method to be successful, and so a 24-gauge sheet metal web was brazed into slots cut in the booms: the unequal heating occasioned by this process caused considerable pre-buckling of the web.

PART IV. COMPARISON OF THE ANALYSES OF THE PRESENT PAPER WITH OTHER RECENT WORK†

11. Taylor's (1949) analysis

By considering the web as shear-carrying only and from the equations for compatibility of displacement at the web-boom junction, Taylor obtains the bending moment in each flange at the loading section due to two equal and similar flange loads W as

$$M_{b_0} = \frac{W}{2}\left(1-\frac{2I_b}{I}\right)^2\left(\frac{h}{h+a}\right)\left\{\frac{EI_b}{Gt_w h}\left(1+\frac{I_b}{A_b(a+h)^2}\right)\right\}^{\frac{1}{2}}, \tag{141}$$

which reduces for $a = 0$, $A_b = \infty$ to

$$M_{b_0} = \frac{W}{2}\left\{\frac{2(1+\nu)\,I_b}{ht_w}\right\}^{\frac{1}{2}}. \tag{142}$$

Our expression for the bending moment (from § 7) is

$$M_{b_0} = W\int_0^\infty \frac{1}{\pi t_w}\frac{\left\{\frac{(1+\nu)(3-\nu)}{2}\coth\alpha h+\frac{(1+\nu)^2}{2}\frac{\alpha h}{\sinh^2\alpha h}\right\}\frac{\alpha I_b}{t_w}}{1+\left\{\frac{(1+\nu)(3-\nu)}{2}\coth\alpha h+\frac{(1+\nu)^2}{2}\frac{\alpha h}{\sinh^2\alpha h}\right\}\frac{\alpha^3 I_b}{t_w}}\,\mathrm{d}\alpha, \tag{143}$$

which reduces for small values of h to

$$M_{b_0} = W\int_0^\infty \frac{1}{\pi t_w}\frac{2(1+\nu)\frac{I_b}{t_w h}}{1+2(1+\nu)\frac{\alpha^2 I_b}{t_w h}}\,\mathrm{d}\alpha$$

$$= \frac{W}{2}\left\{\frac{2(1+\nu)\,I_b}{ht_w}\right\}^{\frac{1}{2}}. \tag{144}$$

We thus see that Taylor's analysis is equivalent to ours provided h is small. For large values of h our analysis tends to that for the flange resting on a semi-infinite plate; Taylor's value of M_{b_0} tends to zero. The difference is shown in figure 27.

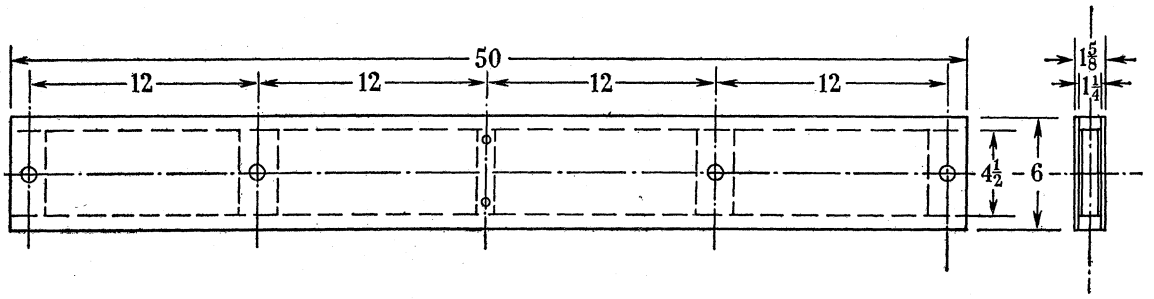

Figure 41. Taylor's wooden beam. Spruce booms, birch ply webs, 10 g mild-steel plates glued to webs at loading points.

In his report, Taylor quotes experimental results for the wooden beam in our figure 41. He applied his theory to this beam and found certain incompatibilities between the experimental and calculated results which he attributed to the finite width of the loading plates.

† Acknowledgement is made to the Chief Scientist, Ministry of Supply, for permission to publish these extracts and figures. Crown copyright reserved. Reproduced by permission of the Controller, H.M. Stationery Office.

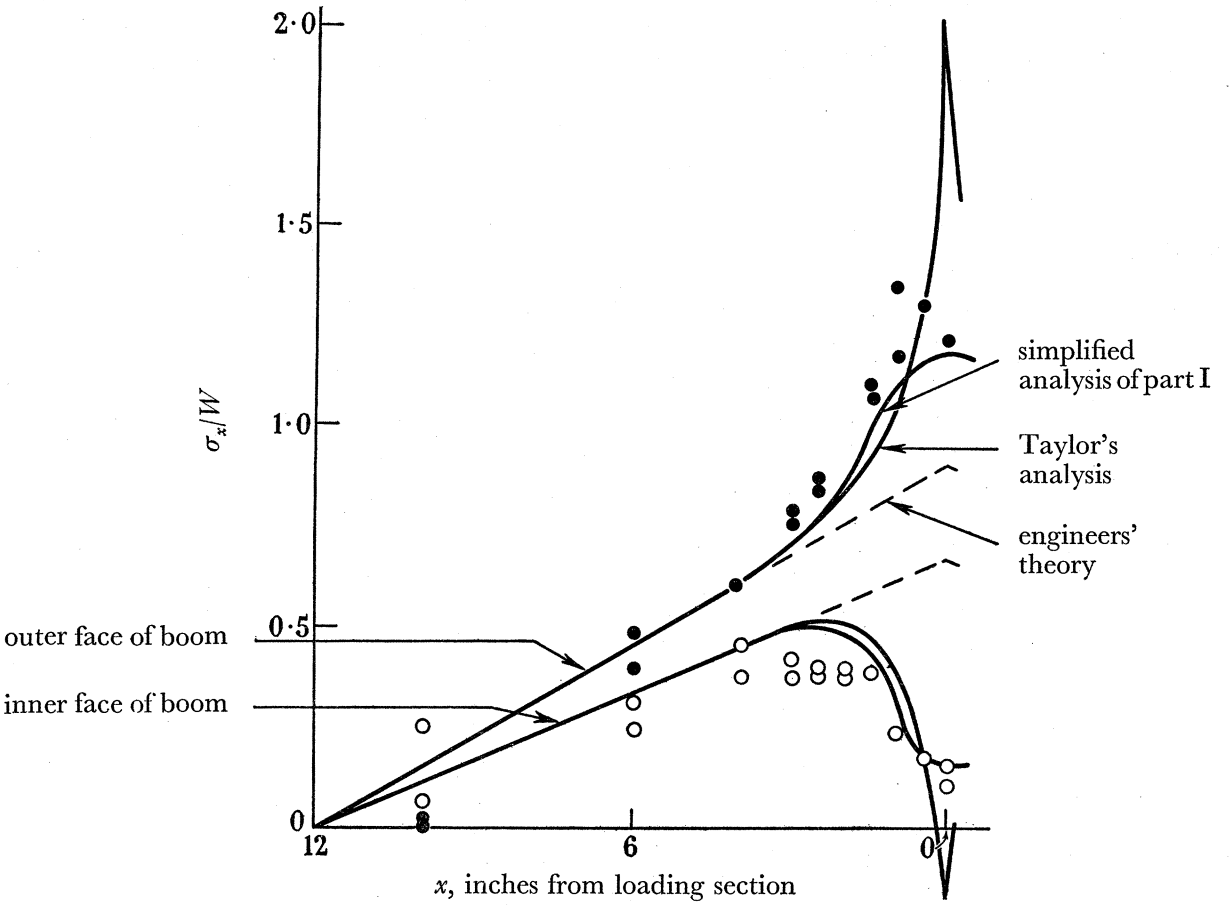

FIGURE 42. Taylor's experimental results, $L/h = 5{\cdot}33$.

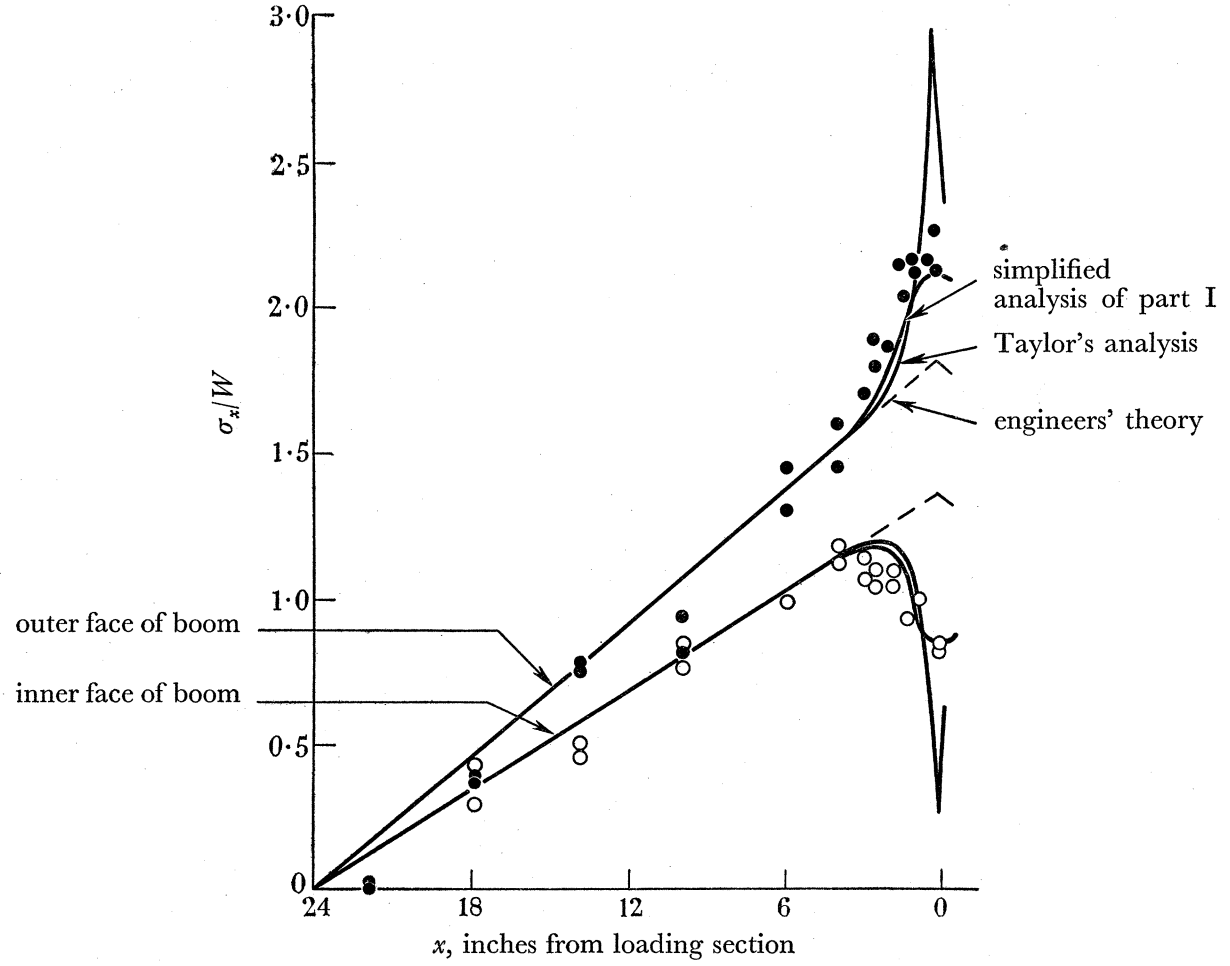

FIGURE 43. Taylor's experimental results, $L/h = 10{\cdot}67$.

By applying the theory of part I of the present paper to the wooden beam, we get quite good agreement between the predicted and experimental stresses, and it seems more likely that Taylor's discrepancies were due to his applying a theory for flange loading to a beam in which load was actually applied to the web (figures 42 and 43).

12. Winny's (1950) analysis

In Winny's analysis, some attempt is made to allow for vertical compression of the web and for rivet slip at the web-boom junction. Both of these quantities are presumed to be proportional to the local vertical loading between web and boom and equations are obtained for compatibility of displacement at the junction. As in Taylor's analysis, the web is assumed to carry shear only and the distribution of load between flanges and web at the loading section depends on the geometry of the section and the coefficient of rivet slip. The area of the boom is assumed infinite and the distance between its neutral axis and the rivet line, zero.

Winny obtains the bending moment in a flange at the loading section due to a load $2W$ as

$$M_{b_0} = \frac{W}{2}\sqrt{\left(\frac{K}{1+K}\right)}\left\{\frac{2(1+\nu)\,I_b}{ht_w}\right\}^{\frac{1}{4}}, \tag{145}$$

where

$$K = \sqrt{(kEI_b)}/2t_w hG, \tag{146}$$

and k is the sum of the compressibility of the web and rivet slip in Lb./in.^{2}. As would be expected, when k is very large, this solution reduces to the same form as Taylor's for $a = 0$, $A_b = \infty$.

Winny quotes a numerical example in which

$$\left.\begin{aligned} 2W &= 14000\,\text{Lb.} \\ h &= 6\,\text{in.} \\ t &= 0{\cdot}064\,\text{in.} \\ I_b &= 3{\cdot}5\,\text{in.}^4 \\ E &= 10{\cdot}5\times10^6\,\text{Lb./in.}^2 \\ G &= 3\times10^6\,\text{Lb./in.}^2 \end{aligned}\right\} \tag{147}$$

The compressibility of the web, assuming the stress to vary linearly to zero at the neutral axis, is $4{\cdot}5\times10^{-6}$ in./Lb./in.; the rivets are $\frac{3}{16}$ in. snap head at $\frac{1}{2}$ in. pitch, giving a coefficient of slip of 3×10^{-6} in./Lb./in. (Parkes 1947), whence $k = 133000$ Lb./in.^{2} and $K = 0{\cdot}96$.

Substituting in equation (145) we get

$$M_{b_0} = 13800\,\text{Lb.in.} \tag{148}$$

By modifying the analysis of part II of the present paper to take account of rivet slip we find that for flange loading

$$M_{b_0} = 18300\,\text{Lb.in.} \tag{149}$$

The discrepancy between equations (148) and (149) is almost entirely due to the fact that Winny's analysis leads to a distribution of load between flanges and web which is dependent on the geometry of the section. The proportion of load carried by the web increases with increase of the coefficient of rivet slip and, as may be seen from equation (145), M_{b_0} decreases. For the case when load is applied entirely to the flanges, we do not find this to be so; according to our analysis M_{b_0} increases with increase of rivet slip.

References

Biot, M. A. 1937 Bending of an infinite beam on an elastic foundation. *J. Appl. Mech.* **4**, 1.

Davies, O. L. 1949 *Statistical methods in research and production.* London: Oliver and Boyd.

Filon, L. N. G. 1903 On an approximate solution for the bending of a beam of rectangular cross-section under any system of load, with special reference to points of concentrated or discontinuous loading. *Phil. Trans.* A, **201**, 63.

Hendry, A. W. 1949 The stress distribution in a simply supported beam of I-section carrying a central concentrated load. *Proc. Soc. Exp. Stress Anal.* **7**, no. 2, 91.

Hildebrand, F. B. & Reissner, E. 1942 Distribution of stress in built-in beams of narrow rectangular cross-section. *J. Appl. Mech.* **9**, 108.

Parkes, E. W. 1947 *Rivet slip and the flexure and torsion of box beams.* Hawker Aircraft, Report no. 1138.

Taylor, J. 1949 *Stresses in built-up beams due to an abrupt change in shear stress at a loading section.* Royal Aircraft Establishment, Report no. Structures 48.

Winny, H. F. 1950 A note on the bending moment induced in the booms of a spar at the point of application of a concentrated load. *Aero. Quart.* **1**, 281.

PHILOSOPHICAL TRANSACTIONS OF THE ROYAL SOCIETY A MATHEMATICAL, PHYSICAL & ENGINEERING SCIENCES